THESIS

EFFECT OF ENDOTHERMIC REACTIONS ON THE GLOBAL EXTINCTION STRAIN RATE OF LARGE HYDROCARBON FUELS

Submitted by

Anish Jadhav

Department of Mechanical Engineering

In partial fulfillment of the requirements

For the Degree of Master of Science

Colorado State University

Fort Collins, Colorado

Fall 2018

Master's Committee:

Advisor: Bret C. Windom

Todd Bandhauer
Mahmoud Hussam

ABSTRACT

EFFECT OF ENDOTHERMIC REACTIONS ON THE GLOBAL EXTINCTION STRAIN RATE OF LARGE HYDROCARBON FUELS

When a hydrocarbon fuel is used as a coolant, the extreme environment can have a significant impact on the fuel composition. Heat exchange occurs through phase change, sensible heat extraction, and endothermic reactions experienced by the liquid fuel. From previous studies it has been demonstrated that the fuel composition changes significantly as well as the fuel properties as a result of the endothermic reactions. To investigate the effect of endothermic reactions on the fundamental flame behavior we have developed a counterflow flame burner that can measure the flame extinction strain rate of a thermally stressed fuel. The counterflow flame burner is coupled with a high-pressure reactor, capable of exposing the fuel to extreme conditions of 170 atm and 650 °C. Flame robustness is quantified by measuring the flame extinction strain rate. n-heptane is studied as a first attempt to understand the role of the endothermic reactions on the combustion and flame behavior of a liquid rocket propellant fuel. Modeling of the reactor and the counterflow flame is carried out using CHEMKIN. The flame extinction strain rate of the reacted n-heptane is compared with the unreacted n-heptane flame, thus allowing us to determine and extrapolate the role of endothermic reactions on the combustion behavior of jet and rocket fuels.

ACKNOWLEDGEMENTS

I would first like to thank my thesis advisor Dr. Bret Windom, the door to his office was always open whenever I ran into trouble or had as question about my research or writing. He steered me in the right direction whenever he thought I needed it.

I would also like to thank Radi Alsulami for helping me with the experimental setup.

Finally, I must express my very profound gratitude to my parents and to my friends for providing me with unfailing support and continuous encouragement throughout my years of study and through the process of researching and writing this thesis. This accomplishment would not have been possible without them.

TABLE OF CONTENTS

LIST OF TABLES

LIST OF FIGURES

CHAPTER 1: INTRODUCTION AND PREVIOUS WORK

1.1 MOTIVATION

Thrust and efficiency of a rocket is proportional to the temperature of the gas prior to its expansion through the nozzle. The gas temperature is limited by the thermal stability of the materials which make up the combustor and nozzle[1]. Combustion temperatures can reach up to 3500 K in the thrust chamber, causing heat fluxes of up to 160 MW/m^2 and thus requires special cooling techniques for the engine[2]. As such, the performance of liquid propellant rocket engines can be enhanced by active cooling of the components near these regions of high gas temperatures. Regenerative cooling, in which the liquid fuel is used as a coolant, is the most commonly used cooling method in the liquid rocket engines. By using the liquid fuel as the coolant, as in regenerative cooling, there is no need for additional coolant and hardware payloads. In a regenerative cooling application, the fuel enters through the micro-channels machined in the walls surrounding the combustion chamber, nozzles and underneath the heat affected exterior areas. From these areas the fuel absorbs the heat, and as a result can lead to the endothermic reactions or decomposition of the fuel. Figure 1.1 shows a simple schematic of a cross section of regeneratively cooled combustion chamber along the axis of a rocket engine. The energy absorbed by the fuel when used as a coolant prior to being combusted can enhance the initial energy content of the liquid fuel prior to injection into the combustion chamber. Due to the increase in the enthalpy of the fuel and the increase in allowable combustion temperatures due to regenerative cooling, improvements in the efficiency of the engine may be realized.

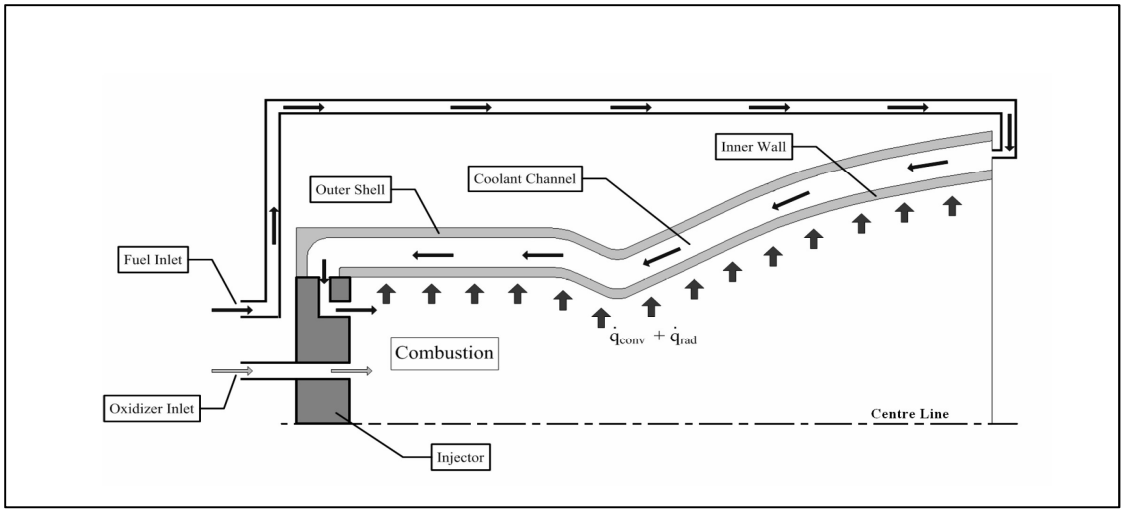

Figure 1.1: Regenerative cooling of a rocket engine[4]

The heat sink of Jet A fuel, which is a kerosene type fuel, is 135 Btu/lb (314 kJ/kg) when heating from 100° to 350°F (38° to 177 °C). If the temperature limit of Jet A fuel were extended, this heat sink would increase to 485 Btu/lb (1127 kJ/kg) at 800°F (427 °C) and 500 psia (3.45 MN/m^2), and to 685 Btu/lb (1592 kJ/kg) at 1000°F (538 °C). This increase in heat extraction at higher temperatures happens due to thermal decomposition of the fuel, which is a highly endothermic process. This additional heat sink increases considerably the cooling that can be accomplished in a rocket engine[5].

The heat absorbed by the fuel during the regenerative cooling is due to sensible heat and latent heat exchange and by way of endothermic reactions which occurs during thermal decomposition of the fuel. For example, 1 kmol of decane can absorb 82 MJ/kmol of energy (including sensible, latent, and chemical heat extraction). To achieve the same cooling capability through sensible heating of 1 kmol of air, a temperature difference of ~2800 K would be needed.

Studies have shown that to obtain sufficient cooling, we can use the endothermic effect which is produced by the thermal reforming of the liquid fuel into lighter components. Figure 1.2 shows how the decomposition of fuel can increase the thermal absorption capacity[6].

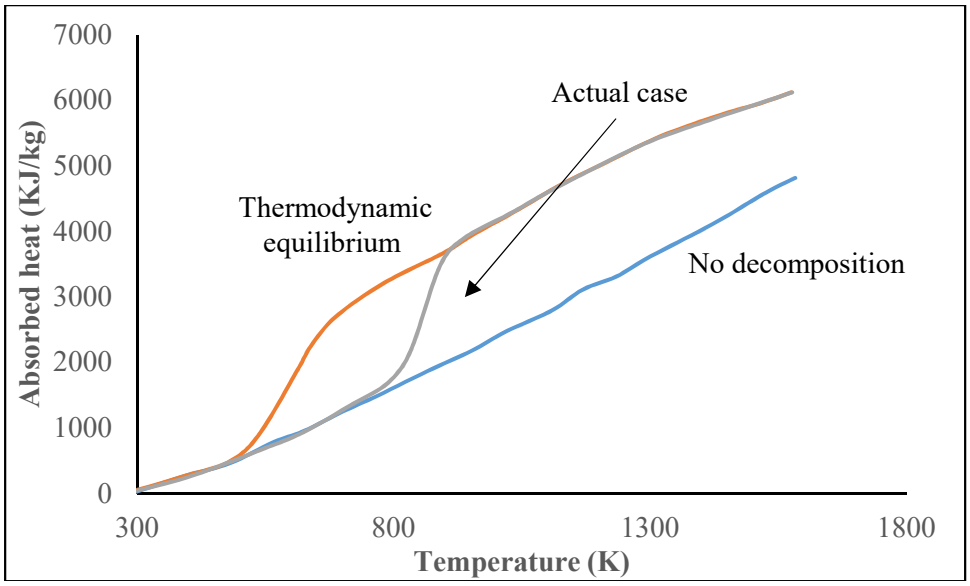

Figure 1.2: Endothermic effect of jet fuel[6]

During the process of heat absorption, the fuel experiences a degree of decomposition. The change of composition of the fuel can in turn have an effect on the combustion stability. The hydrocarbon fuel cracks into smaller chains of stable species. Hydrocarbon cracking is a process in which the higher molecular weight hydrocarbons are converted into the lower molecular weight hydrocarbons through C-C bond fission. From this arises a question: how does the fuel decomposition that occurs in a regenerative cooling application effect the combustion performance and stability and how does this affect impact surrogate fuel formulation and the development of combustion mechanisms needed to predict and design future engines that rely on regenerative cooling? To help answer these questions, the present study will investigate the amount of thermal decomposition a fuel can experience and the effect of this decomposition on the stability of a counterflow diffusion flame. n-Heptane and to a lesser extent n-dodecane are tested using a high temperature. High pressure reactor to thermally stress the fuels before quantifying their flame stability using a counterflow flame burner. Both the thermal decomposition and the flame stability

are predicted using current state of the art chemical mechanisms to evaluate their ability in predicting this complex phenomenon.

1.2 BACKGROUND

The concept of regenerative cooling has been studied for years[7,8,9]. In fact, regenerative cooling is often applied in rocket engine operation, most of the time when cryogenic fuels (H_2/O_2) are used[9]. For air breathing propulsion applications (and many rocket/missile applications), where it is necessary to use high energy density fuels (without having to use cryogenic systems to cool them to liquid state), liquid hydrocarbon fuels are desired. Hydrocarbon fuel is used in a regenerative cooling because of simplicity of fuel handling and storage, and cost savings[10]. Regenerative cooling using liquid hydrocarbon fuels presents added challenges, but also significant benefits as described in the previous section. Though one can take advantage of the additional heat capacity of the fuel when used as a coolant by allowing for the fuel to stress and undergo endothermic reactions, this can also lead to coking and fouling of the cooling channels which can restrict fuel flow and become catastrophic to the propulsion system. As such, a number of studies have been performed exploring different combinations of fuel types and micro-channel designs, including catalytic surfaces, on regenerative cooling applications[11,12].

Jiang et al.[13] used regenerative cooling channels to find the thermal cracking behavior of the endothermic hydrocarbon fuels using an electrically heated tube. The pyrolysis of the Jet-A fuel was done at 5 MPa, over a temperature range of 680 °C- 700 °C, the mass flow rates were from 0.4 -1 g/s, and the inner diameter of the tube was 1 mm. The author used these conditions to find the local chemical composition of the thermally stressed hydrocarbon fuel along the length of the cooling microchannels. The work by the author also produced development of a new molecular reaction model consisting of 18 species and 24 reactions to predict the thermal cracking of the

hydrocarbon aviation fuel for supercritical conditions. A similar work of experimental and modeling of pyrolysis using n-decane as a fuel at supercritical pressures was done by Jia et al[14]. The experiments were conducted at pressures of 3, 4, and 5 MPa over a temperature range from 773 K to 943 K. A sensitivity analysis was also done by the author to identify the influences of the reactions on the concentration of specific species. The main products identified during the thermal decomposition were alkenes and alkanes. The total mole fraction of the alkanes was 1/3rd of that of the pyrolysis products, meaning a lot more unsaturated compounds were formed. The kinetic model based on the experimental results consisted of 164 species and 842 reactions. The author had a satisfactory agreement between the modeled kinetic mechanism for n-decane and the experimental results. Jiao et al.[15] used n-decane as a fuel to study the effect of supercritical pressures on the thermal cracking. The author conducted the study at various pressures of 3, 4, and 5 MPa. The experimental condition used by the author followed the Jia et al work. From this study a molecular kinetic model was proposed by modifying the Kumar-Kunzru kinetic model for n-decane pyrolysis. The author's work helped to get a better understanding on thermal cracking of fuel in a regenerative cooling channel. Windom et al.[17] measured the change of composition of common hydrocarbon rocket propellants (RP-1 and RP-2) following thermally stressing the fuels and showed that the change in composition could result in significant changes to key thermo-physical properties of the fuel including molecular weight, speed of sound, viscosity, density, and volatility[16,17].

Much of the work to date in the field of regenerative cooling has been focused on the heat transfer mechanisms and the effect of this heat transfer on fuel composition, however, only recently have studies been performed exploring the endothermic reactions of jet fuels at engine relevant pressures (greater than 100 atm) and temperatures (greater than 850 K). Despite much of this

previous work, there is a need to predict the thermal decomposition of these fuels as well as their supercritical thermal transport phenomenon at relevant pressures and temperatures. To this end, there is a need for carefully designed controlled high pressure and high temperature reactor experiments which can produce repeatable composition data to validate chemical mechanisms and reactor simulations. Finally, there is a need to understand and predict how the endothermic reactions impact the combustion and flame dynamics. Given that there is a reduction in molecular weight and the production of more unsaturated hydrocarbons one may expect to see improvements in the flame stability, however, to date, there has been very limited work done in this field[13,14,15]. As such, there is also a need to evaluate current chemical mechanism and their ability to predict both the thermal decomposition but also the impact of these reactions on key flame behaviors. To this end, data from carefully described experiments capable of being modeled with high accuracy are needed.

The development of chemical kinetic mechanisms capable of predicting the thermal decomposition of the fuel is a key component in simulating a hydrocarbon fueled regeneratively cooled propulsion system. In the past few decades, the pyrolysis, oxidation and combustion of n-heptane has been extensively studied. Pant et al.[18] studied the pyrolysis of n-heptane using a tubular flow reactor at atmospheric pressures and higher pressures. The products identified were methane, ethylene, propylene, 1-butene, 1-pentene, and 1-hexene. Garner et al.[19] also did a study using saturated and unsaturated heptane hydrocarbons. The experimental pressure for the pyrolysis experiments ranged from 25 to 50 atm and the temperature varied from 1000 to 1350 K with the reaction ranging from 1 to 3 ms. The major species obtained through pyrolysis were acetylene, ethene, ethane, propene, allene, propyne, 1-butene, and 1,3 butadiene. In their study it was found that there was no pressure dependency on n-heptane decay and acetylene formation, indicating that

the reactions were at high pressure-limit. Another study of pyrolysis of n-heptane at 3.95 atm and a temperature range of 900-1500 K was done by Fridlyand et al[20]. The species identified by Fridlyand were methane, ethylene, acetylene, and propylene. It should be noted that the species identified by Garner and Fridlyand are typical hydrocarbon species that are burned within the combustion chamber of a hypersonic vehicle. It should be noted that the majority of the studies exploring pyrolysis of these simple fuels have been carried out at high temperatures but often at lower pressures than those potentially experienced in an actual hypersonic regenerative cooling application.

One of the most used combustion platforms to study the influence of fuel chemistry and transport phenomenon on diffusion flame stability is a counterflow flame burner. These platforms are used to measure the flame extinction behaviors for both gaseous and liquid fuels. One of the first applications, by Potter and Butler[21], used two vertically opposed jets of oxidizer and fuel to study the experimental extinctions of various gaseous fuel. A counterflow flame was stabilized in between the two nozzles. By increasing the flow rates of both fuel and oxidizer they found that the flame extinguished at a certain flow rate. In literature there was no means of quantifying flame extinction, so Porter et al. used the mass flow rate per unit area to measure the extinction strain rate at the point of extinction. The nozzles used by the author were converging which gave a uniform flow profile, also the authors observed that the extinction strain rate varies with changing the distance between the two nozzles. Basically, a counterflow flame burner creates a circular flame that can be approximated as 1-dimensional allowing one to model the fluid dynamics and flame chemistry using semi-detailed chemical mechanisms. These burners are now used in many laboratories to evaluate chemical mechanisms and derive surrogate fuels to be used in computer aided engineers applications of state of the art engines. For example, Dooley et al.[22] used

counterflow flame burner to calculate the extinction strain rates of Jet A and compared it to a surrogate mixture of n-decane, toluene and iso-octane. The author chose these three hydrocarbons in order to represent the hydrogen/carbon ratio of Jet A. The surrogate mixture was having good agreement with the measured extinction strain rate of Jet A fuel. Dooley concluded that the surrogate mixture was an accurate representation of Jet A in practical combustion systems. There are additional studies regarding the combustion properties of a surrogate fuels that emulate the behavior of neat jet fuel[23,24,25]. Nevertheless, no one has done a study on fuel surrogates that would match the high-pressure pyrolysis and combustion properties of a fuel after it has been used in an endothermic cooling system.

1.3 DEFICIENCES IN LITERATURE

Summarizing the literature, we can say previous work was mainly focused on identifying the composition of the stressed fuel at various temperatures and pressures (limited to 50 atm). In addition, relevant previous work has focused on the heat transfer mechanism and its effect on the composition of the fuel, but little work has been carried out coupling the thermal decomposition phenomenon of the fuel during regenerative cooling and its impact on the combustion. Furthermore, previous work has not explored the influence of the thermal decomposition on the derivation of surrogate fuels, whereas most of this work has focused on carrying out fundamental combustion experiments on propulsion fuels to identify surrogate fuels based on the reproduction of combustion chemical kinetics, transport, and physical properties of the real fuels.

The majority of previous work investigating the thermal decomposition of hydrocarbon surrogate/real fuels have often carried out experiments at pressures less than 50 atm which is less than pressures experienced by most fuel delivery systems. The current study will be carried out at extreme pressures (up to 170 atm) which may emulate the injection pressure condition inside a jet/rocket engine after the fuel has been pyrolyzed. Due to this extreme pressure and temperature the fuel will experience different levels of decomposition. As such, this study will be the first to evaluate current chemical mechanisms ability to predict fuel decomposition at these extreme conditions. Furthermore, the current study will couple the effect of thermal decomposition on the flame extinction behavior of hydrocarbons that found in liquid propulsion fuels. This work will ultimately help design and validate new chemical kinetic mechanisms and surrogate fuels that can be used in the computer aided engineering of future regeneratively cooled propulsion systems.

1.4 OBJECTIVES

The reminder of the thesis will describe the work that has gone into addressing the following project objectives:

1. Commission an existing counterflow flame burner and validate the measurement approach using a methane flame and comparing data with previous results.
2. Build a controllable high-pressure reactor that mimics the thermal decomposition of a fuel such that it provides the best representation of a regenerative cooling system seen in rocket/high speed propulsion systems.
3. Monitor the change of fuel composition when exposing n-heptane and n-dodecane in the high-pressure reactor while varying pressures and temperatures up to 170 atm and 923 K, respectively.
4. Study the effect of endothermic reactions on the extinction strain rate by coupling the high-pressure reactor with a counterflow flame burner.
5. Model the thermal decomposition of the fuel using a plug flow reactor to predict the extent to which the fuel experiences decomposition and compare these predictions to those measured in the experiments.
6. Quantify flame stability through the measurement of the flame extinction strain rate for unreacted and reacted n-heptane and n-dodecane.
7. Determine the flame extinction strain rate using the OPPDIF module of CHEMKIN package and compare these results to measured values. Using a published alternative approach, explore the feasibility of predicting extinction strain rates of the decomposed fuels without the need of complex counterflow flame kinetic calculations.

1.5 THESIS OUTLINE

The organization of the thesis is outlined below:

Chapter 2 provides a brief overview of the relevant combustion fundamentals utilized in this study. The first section outlines the basics of the combustion terms that will be used throughout the thesis. The subsequent sections describe the modeling of the reactor and the counterflow flame burner including a discussion regarding the modules that are used for simulation and the conservation equations that are solved.

Chapter 3 describes the experimental set-up of the high-pressure reactor and the counterflow flame burner along with a description of the experimental measurements used throughout. The methods applied to quantify the composition of the stressed fuel using GC/FID are also presented.

Chapter 4 reviews the detailed and reduced chemical kinetic models that are used to compare the reactor and burner experiments. The chapter outlines the numerical modeling process required to simulate the conditions at which the experiments are completed.

Chapter 5 presents the experimental results for the various conditions investigated in the reactor and burner and compares them with the predicted results from the simulations. Species composition and counterflow flame data are presented for a range of reactor pressures and temperatures.

Chapter 6 concludes the outcomes of the study and gives some ideas about the future work.

CHAPTER 2: COMBUSTION THEORY

This chapter describes the combustion concepts that are used throughout this study. Flame dynamics, including laminar and turbulent flames, flame stretch, strain rates, flame extinction, and counterflow flame burner theory are discussed in detail. Lastly, a description of the numerical modeling, including the equations that are used in prediction of thermal decomposition through a plug flow reactor (PLUG), and counterflow flames (OPPDIF) is provided.

2.1 INTRODUCTION

The combustion process has been a topic of interest for many years as it has a significant impact on our daily lives. The combustion of fossil fuel produces about 85% of the world's total energy. But it also has severe negative impact such as global warming, depletion of natural resources etc. It is responsible for the emission of the nitrogen oxides (NOx), carbon monoxide (CO), particulates (soot and aerosols), and other products that affect the human health and environment. There has been tremendous efforts by the pollution control agencies, environmental protection agencies and also the vehicle manufacturing companies to limit the emissions. In order to do this, it has been increasingly difficult to produce high efficiency and low emissions from combustion devices.

To develop high performance jet engines, predictive models including the fundamentals of combustion such as flame propagation, ignition and extinction of flames should be developed. This study is focused on fundamental combustion and flame phenomenon. Experimental and numerical modeling approaches are used to investigate the effect of thermally stressed fuel on the flame extinction behavior.

2.1.1 Combustion concepts

A flame is defined as a self-sustaining propagation of a localized combustion zone at subsonic velocities[26]. The distinguishing feature of a flame is that it is a localized reaction zone which is able to self -propagate through gaseous mixture that support it. The flame is divided into four zones: unburned gas zone, preheat zone, reaction zone, and burned gas zone. When the mixture reaches the flame front, it is heated by conduction and radiation from the flame zone upstream. The heat release and chemical reactions are negligible in the preheat zone. Once the temperature of the reactants has reached the level to sustain combustion, chemical reactions takes place in the reaction zone. The gases emerging from the reaction region enter the burned gas zone where their temperatures and concentrations reach equilibrium values post flame.

2.1.2 Flame types

The flames are classified into three categories: premixed flames, diffusion flames (non-premixed) and partially premixed flames[19]. Premixed flames are those flames in which fuel and oxidizer are mixed prior to chemical reaction, these flames typically need high ignition temperature to initiate. The burning rate is controlled by diffusion and chemical reactions. We find premixed flames in Spark Ignition engines and Gas Turbine engines. Diffusion flames are those flames in which the fuel and oxidizer are initially separated, and the chemical reactions occurs at the interface between the two reactants. It is characterized by an exothermic process, and the burning rate is controlled by the rate of mixing of the fuel and the oxidizer. These flames are found in the diesel engines and also jet engines. The burning process in diffusion flames depends more upon the rate of mixing rather than the rates of the chemical processes involved as the chemical reaction rate is much faster than the diffusion velocity of the gas. In diffusion flames the chemical reaction occurs in a narrow zone between the fuel and the oxidizer often referred to as the flame

sheet model, where the concentration of fuel and oxidizer are very low chemical kinetics are considered infinitely fast and the combustion rate is solely controlled by the rate at which the fuel and oxidizer flow into the reaction zone[27].

Flames are also classified by the flow patterns in which they interact, namely laminar and turbulent flames. In general, laminar flames are predictable and smooth. They have been studied extensively as they provide the most detailed information about combustion chemistry and various effects that act upon the flame. Turbulent flames on the other hand are unpredictable and chaotic. They introduce more mixing of the fuel and the oxidizer due to generation of small turbulent eddies. They are found in most combustors. Laminar flames are easier to study because of the non-turbulent behavior and the ability to model/predict the fluid dynamics that act on the flame.

2.1.3 Flame sheet and flame stretch

The first detailed analysis of flame sheet model was given by Burke and Schumann in 1928. They were able to predict the flame's height and shape, thus making it very useful for the study of laminar diffusion flame. In flame sheet model:

1. The reaction zone is infinitesimally small by assuming that the combustion kinetics are infinitely fast (as compared to the mixing time scales) and, the combustion region becomes a flame sheet,
2. At the flame surface the concentrations of fuel and oxidizer become zero, there is no fuel present on the oxidizer side and no oxidizer present on the fuel side, and
3. The diffusion rates of transport of fuel and oxidizer to the flame surface must be in stoichiometric proportions. That is the flame will always be located near the stoichiometric mixture fraction in accordance of the second law of thermodynamics.

The concept of flame stretch was first introduced by Karlovitz in 1953 to describe flame extinction under the influence of velocity gradients[28,29]. The amount of stretch a flame experiences on its surface due to curvature and outer velocity field strain is quantified as flame stretch[30]. The Karlovitz number was defined as[31]:

$$K_a = \delta \frac{1}{u} \frac{du}{dx} \tag{2.1}$$

where δ is a measure of the flame thickness, and u the axial flow velocity along the x-dir[31,32]. The Karlovitz number is defined as the ratio of the convective timescale to the chemical timescale[9,10].

This concept was used by Lewis and von Elbe in 1961 to explain and quantify phenomena associated with flame stabilization[32]. They offered explanations of many combustion phenomenon with simple idea that flame stretch slows a flame and a sufficient large amount of stretch can extinguish a flame[33]. Recent studies noticed that the definition of flame stretch given by Karlovitz was not true for the case of spherically expanding flame for which the flow is uniform, that is, one-dimensional, but the stretch is not zero.

A much more generalized definition of flame stretch was given by Forman Williams, which can be described by the equation[32] (2.2),

$$K = \frac{1}{A} \frac{dA}{dt} \tag{2.2}$$

where A is the area that belongs to the flame surface, has the same normal velocity as the flame surface, and has the same tangential velocity as the surrounding flame

The Figure 2.1 represents a thin sheet, which is moving at $\underline{V}$ velocity and is surrounded by fresh gas at the velocity $\underline{v}$[32]. The flame is strained in both normal and tangential direction.

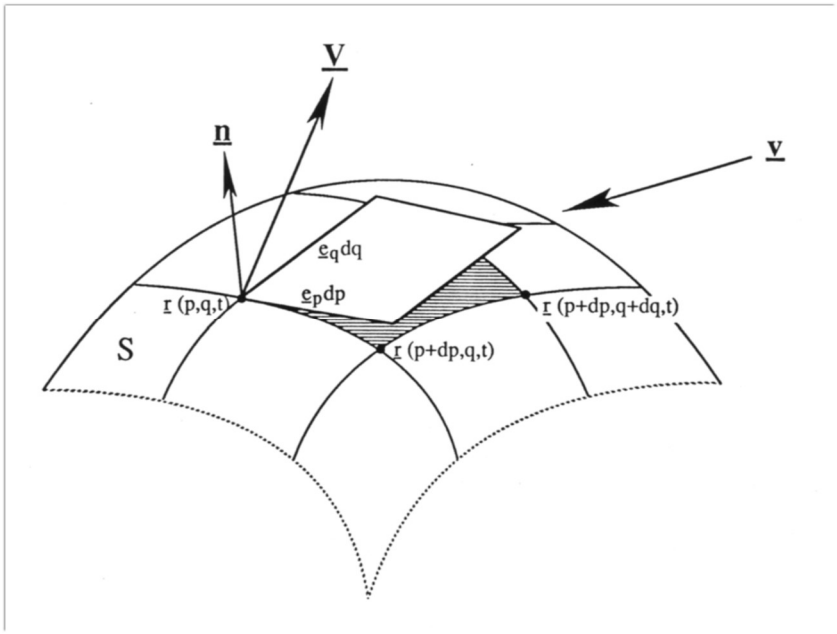

Figure 2.1: An isotherm surface to define flame stretch[32]

2.2 Strain Rate

Extinction strain rate is an important combustion characteristic for diffusion flames[33]. In the reaction zone of non-premixed flame strain rate is measured as the residence time of the reactants in it. Extinction strain is defined as the maximum strain rate (small residence time) that a flame can support just before extinction. Extinction strain rate is a fundamental property of the fuel, it helps in designing and validation of kinetic models[34]. With an increase in the strain rate the residence time decreases, which means the reactants are supplied to the reaction zone faster than these are consumed. This has an effect which reduces the flame temperature, making the reactions slower and eventually extinguishing the flame[35]. The global strain rate (K), based on the relation of Sheshadri and Williams is given by:

$$a = \frac{2v_2}{L}\left(1 + \frac{v_1\sqrt{\rho_1}}{v_2\sqrt{\rho}_2}\right) \tag{2.3}$$

where ρ_1 and ρ_2 represents the density of fuel and oxidizer, respectively, and v_1 and v_2 denotes the velocity of fuel and oxidizer, respectively. The extinction is achieved by increasing the velocity of the fuel while keeping the flow rates of the oxidizer constant. L is the separation distance between the two nozzles. To characterize the influence of strain on the flame, global strain has been adopted in the counterflow flame literature. The velocity of fuel and oxidizer at the nozzle exit are calculated as the measured volumetric flowrates of the reactants divided by the cross-sectional area of the nozzle exit. Further explanation on the measurements will be provided in subsequent chapters.

2.3 Counterflow flame burner

Counterflow burners are used to create symmetrical stagnation-point flows in which combustible mixtures can be ignited and burned. It has been commonly used to study the behavior of stretched flames. Counterflow diffusion flames are classified in two large groups: 1) the counterflow diffusion flame between two opposed jets, one of fuel and one of oxidizer, and 2) the counterflow diffusion flame in the forward stagnation region of a porous burner immersed in uniform oxidizer flow. There is further subdivision of the flames represented by Figure 2.2: I) quasi-flat flame at the impingement of two opposed jets from circular tubes or rectangular nozzles, II) quasi-static flame established between two opposed matrix burners ejecting the individual reactants, III) the flame at forward stagnation region of a spherical or hemispherical porous burner, and IV) flame at the forward stagnation region of cylindrical porous burner[27]. A type 1 counterflow flame is used in this work.

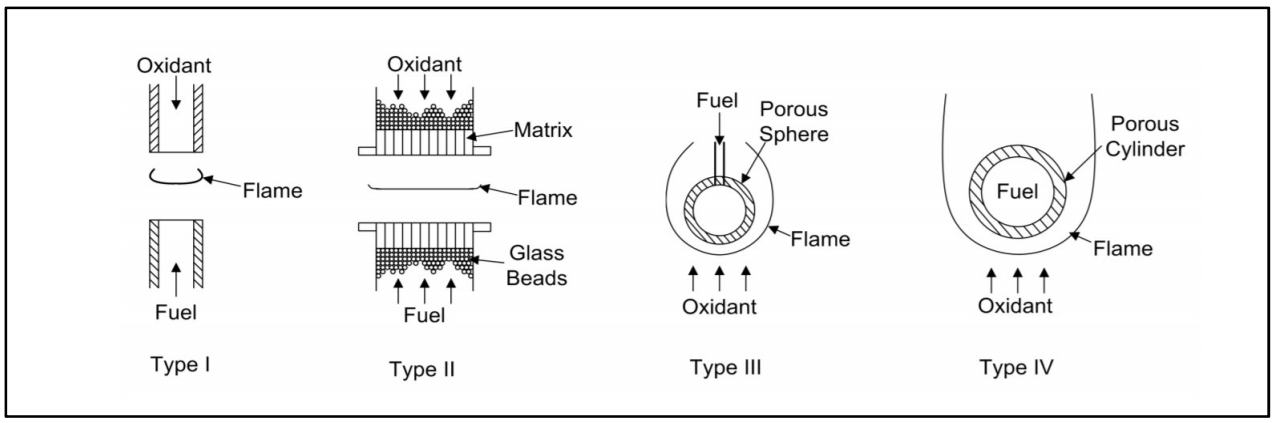

Figure 2.2: Classification of counterflow flame burner[27]

A schematic representation of our counterflow flame burner is given in Figure 2.3. The counterflow flame burner has a fuel side, which of made up of the alkane fuels and nitrogen that is injected towards the mixing layer with a velocity u_f. The other side is the oxidizer stream which is air with an injection velocity of u_o. Adapted from Eqn. 2.3, the strain rate of the fuel is given by the formula,

$$a = \frac{2u_o}{L}\left(1 + \frac{u_f\sqrt{\rho_f}}{u_o\sqrt{\rho}_o}\right) \tag{2.4}$$

The denotation f and o are for fuel and oxidizer. Counterflow flame burners are used in fundamental research as the gradient exist in the axial direction and the flow can be regarded as one dimension along the centerline. Also, because of the symmetry there is a minimum heat loss thus providing a nearly adiabatic stagnation flame.

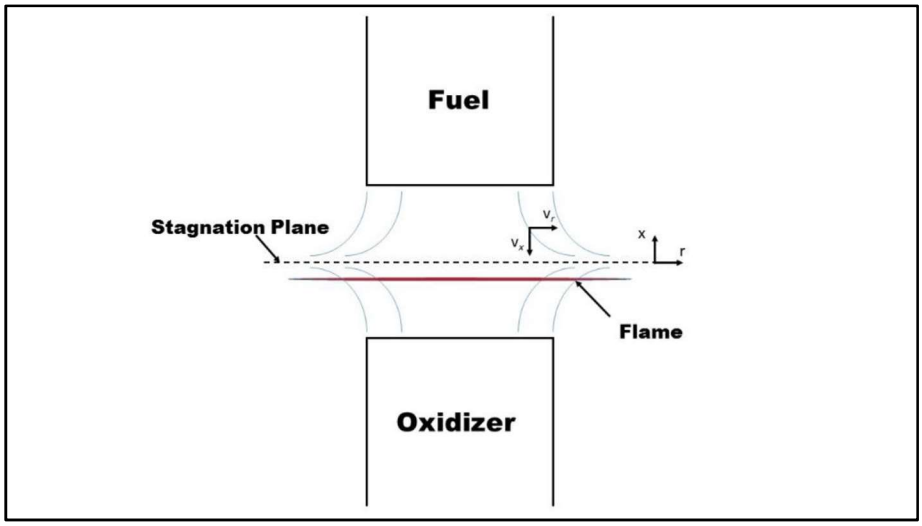

Figure 2.3: Schematic of counterflow diffusion flame burner

The two opposing jets of fuel and oxidizer create a stagnation plane where velocity in the x direction is zero i.e u_x=0. However, even if there is an imbalance in the momentum the flame can be positioned in the center. The location of the flame is dependent on the position where the mixture is nominally stoichiometric[26].

Laminar flames in counterflow flame burner have been studied under various flow and boundary conditions, because of their simple geometry, fundamental flame behaviors and burning properties. S shaped curve is obtained when plotting the maximum flame temperature against the corresponding Damkohler number (D_a) of a reactive system. This phenomenon can be credited to the exponential dependence of the chemical reaction rate on temperature[36,37]. Damkohler number is defined as the ratio of the characteristic residence time to the characteristic chemical time and is used to characterize the intensity of the chemical reaction in a burning flame. The curve represents all the possible steady state a reacting mixture can achieve. It can be used to characterize the evolution of a flame which includes ignition, extinction, and instability. Figure 2.4 shows the S curve of a flame. From figure 2.4, where there is pure mixing of reactants the D_a is zero. This state is called frozen limit. The lower branch if the curve denotes weakly reactive states, the middle

branch denotes the unstable solution, and the upper branch shows vigorous burning rates. The turning points for the lower and upper branches can be defined as the ignition and extinction states of the system.

Auto-ignition is unlikely to happen in open diffusion flames, that corresponds the region of the middle branch i.e. the unstable burning branch, since the required residence time scale is very large. Auto-ignition occurs in the Diesel engines. There is an interdiffusion of the diesel fuel with the surrounding hot air which leads to decreasing mole fraction gradients and thus decreasing dissipation rates[38]. S curve is used to identify the point of extinction in the modeling. More information is given in the next section about it.

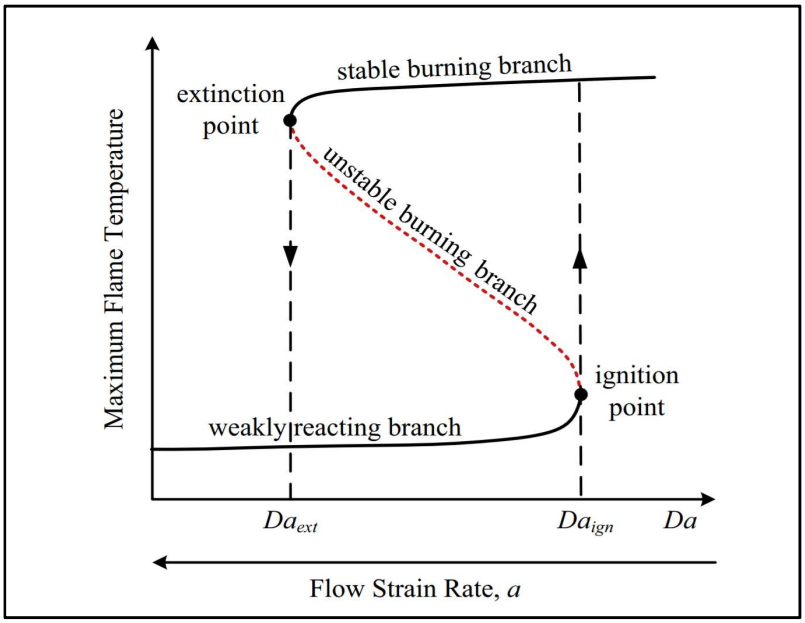

Figure 2.4: S shaped flame response curve[38]

2.4 CHEMKIN Modeling

The numerical analysis of flames was done by using CHEMKIN software, released by ANSYS. It is a tool that allows simulations of complex one-dimensional chemical reactors. CHEMKIN was used to predict the composition of the thermally decomposed fuel, and the extinction characteristics of the alkanes/air diffusion flames. The following modules of CHEMKIN have been used in performing simulations: PLUG[40] and OPPDIFF[40]

2.4.1 PLUG module

The PLUG module is a program in the CHEMKIN package that models an ideal plug flow reactor. The assumptions made while modeling the plug flow reactor are: there is no axial mixing but perfect mixing the direction transverse to the flow, steady state, and non-dispersive[41]. This module is used to find the composition of the thermally stressed fuel. The general equation for chemically reacting flow involves kinetics, thermodynamics and also transport phenomenon. There is a lack of transverse gradients that implies the mass-transfer limitations are absent. The plug flow reactor model uses the first order ordinary differential equations, since no transport properties are needed.

The governing differential equations for the plug flow reactor are simplified versions of the general relations for conservation of mass, energy, and momentum.

Mass continuity equation

$$\rho u \frac{dA}{dx} + \rho A \frac{du}{dx} + Au \frac{d\rho}{dx} = \sum_{m=1}^{M} a_{i,m} \sum_{k=1}^{K_g} \dot{s}_{k,m} W_k \tag{2.5}$$

where ρ is the mass density and u the axial velocity of the gas, which consists of K_g species; W_k is the molecular weight of species k, and $\dot{s}_k$ is the molar production rate of this species by all surface reactions. The quantities A and $a_{i,m}$ are the cross-sectional (flow) area and the effective

internal surface area per unit length of material, respectively, in the reactor. Both A and $a_{i,m}$ can change as arbitrary functions of x. Equation 2.5 simply states that the mass flow rate of the gas can change as a result of generation or consumption by surface reactions on all materials in the reactor and it should be noted, in experiments the surface reactions are ignored.

Gas-species conservation equation

$$\rho u A \frac{dY_k}{dx} + Y_k \sum_{m=1}^{M} a_{i,m} \sum_{k=1}^{K_g} \dot{s}_{k,m} W_k = W_k \left(\sum_{m=1}^{M} \dot{s}_{k,m} a_{i,m} + \dot{\omega}_k A \right) \tag{2.6}$$

Here Y_k is the mass fraction of species k and $\dot{\omega}_k$ is its molar rate of production by homogeneous gas reactions. Such reactions cannot change the total mass of the gas, but they can alter its composition.

Energy equation

$$\rho u A \left(\sum_{k=1}^{K_g} h_k \frac{dY_k}{dx} + \bar{C}_p \frac{dT}{dx} + u \frac{du}{dx} \right) + \left(\sum_{k=1}^{K_g} h_k Y_k + \frac{1}{2} u^2 \right) \sum_{m=1}^{M} a_{i,m} \sum_{k=1}^{K_g} \dot{s}_{k,m} W_k \tag{2.7}$$

$$= a_e Q_e - \sum_{m=1}^{M} a_{i,m} \sum_{k=K_b^f}^{K_b} \dot{s}_{k,m} W_k h_k$$

where is the specific enthalpy of species k, $\bar{C}_p$ is the mean heat capacity per unit mass of the gas, T is the (absolute) gas temperature. In the right-hand summation, $\dot{s}_{k,m}$ is the molar production rate of bulk solid species k by surface reactions on material m. Equation 2.7 states that the total energy (enthalpy plus kinetic) of the flowing gas changes due to the heat flux Q_e from the surroundings to the outer tube wall (whose surface area per unit length is a_E) and also due to accumulation of enthalpy in the bulk solid.

Momentum equation

$$A\frac{dp}{dx} + \rho u\frac{dA}{dx} + \frac{dF}{dx} + u\sum_{m=1}^{M} a_{i,m}\sum_{k=1}^{K_g}\dot{s}_{k,m}W_k = 0 \tag{2.8}$$

where *P* is the absolute pressure and *F* is the drag force exerted on the gas by the tube wall.

2.4.2 OPPDIF module:

The OPPDIF[40] module in the CHEMKIN package computes a numerical model of the opposed diffusion flow flame. For obtaining the S curve we have to first make an initial guess to obtain a solution on the upper branch and then proceed towards the turning point. There is difficulty as the solution approaches the turning point because of the singularity of the Jacobian matrix of the governing equations. To avoid this the temperature at the stagnation plane should be fixed and the inlet velocities will be set as dependent variables. Figure 2.5 shows the geometry of the counterflow flame burner. The dashed line represents the stagnation line, the shaded region suggests the flame. Figure 2.5 shows the geometry of the counterflow flame burner. The dashed line represents the stagnation line, the shaded region suggests the flame.

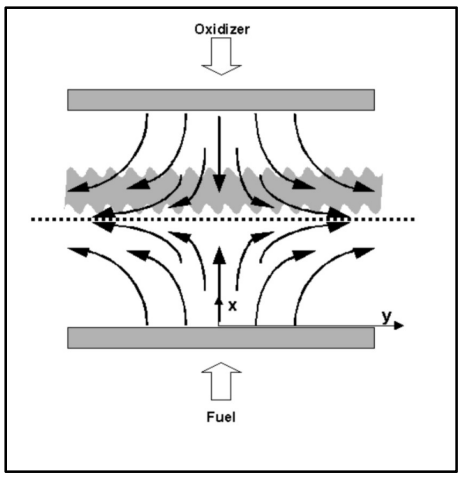

Figure 2.5: Geometry of the planar opposed-flow diffusion flame[40]

A TWOPNT method solves the boundary problem using the Newton iteration method. It is a steady state solver that automatically refines the grid by adding points regions where they

needed to resolve the first and second derivatives of the solution. A TWOPNT method is used to establish a diffusion flame.

2.4.3 Mechanism reduction workbench

To reduce the detailed chemical kinetic mechanism, Reaction Workbench[40] is used. This is needed for the simulation of counterflow flame burner, since detailed mechanism are typically large and computationally expensive to apply in practical simulations. There are several methods that are available in the Workbench to reduce the mechanism such as Directed Relation Graph (DRG), Directed Relation Graph with Error Propagation (DRGEP), linear lumping of isomer species and, Full Species Sensitivity Analysis (FSSA). Of these methods DREGP is used for the reduction of mechanism. The first two method are commonly used, it is advised to use them because the other two methods work best with smaller skeletal mechanism. One of the advantages of using DRGEP over DRG is it eliminates more species. The selection of starting species is important in DREGP because the initial species would be described accurately, and the other species would be adjusted.

Chapter 3: EXPERIMENTAL METHODS

This chapter describes the methods used to obtain the results shown in Chapter 5 of this thesis. The high-pressure reactor system will be described first followed by the experimental techniques for thermal decomposition measurement, and then the burner configuration that is coupled with the high-pressure reactor.

3.1 High Pressure Reactor

The schematic of the reactor that is used to thermally stress the fuel is shown in Figure 3.1. This system consists of three parts. Initially, there is a high-pressure syringe pump (ISCO Model 260D) that is capable of generating 55 MPa, at constant flow rates. The thermal decomposition of fuel is widely studied over the range of 0.7-1.5 mL/min of volumetric flows controlled by the syringe pump. This pressurized fluid is delivered to the high temperature reactor made of 316 stainless steel tube of OD 1/16” and ID of 0.022”. The length of this reactor is 25 cm and is place inside a split tube furnace. It is an Applied Test Systems series 3210 furnace which is made up of stainless-steel shell depicted in Figure 3.2. It is used to thermally stress the fuel. It can reach 950 °C and the heating section is 9 inches in length. The stainless tube had to be coiled in the middle section of the furnace such that it can fit into it. To control the temperature of the furnace an omega PID was used. A K type thermocouple capable of reaching temperatures of 1300K is used to provide the feedback to the PID. The reactor can generate temperature of 950 °C with uncertainties less than ± 5 °C for temperature at 600 °C and ± 7 °C for 650 °C. After passing through the reactor it is passed via a stainless-steel tube to the NESLAB chiller water heat exchanger, model RTE-140, set at 8 °C in order to quench the reaction and cool the thermally stressed fuel. It also avoids the direct contact of the hot fuel with the back pressure regulator (IDEX Health & Science) which

is made of PEEK material. The back-pressure regulator is used to control the pressure of the reactor. The volumetric flow rates of the fuels were controlled using an ISCO® Model 260D high pressure syringe pump. The residence time of the reactor was controlled by specifying the volumetric flow rate of the high-pressure syringe pump. The reactor is then coupled with counterflow flame burner.

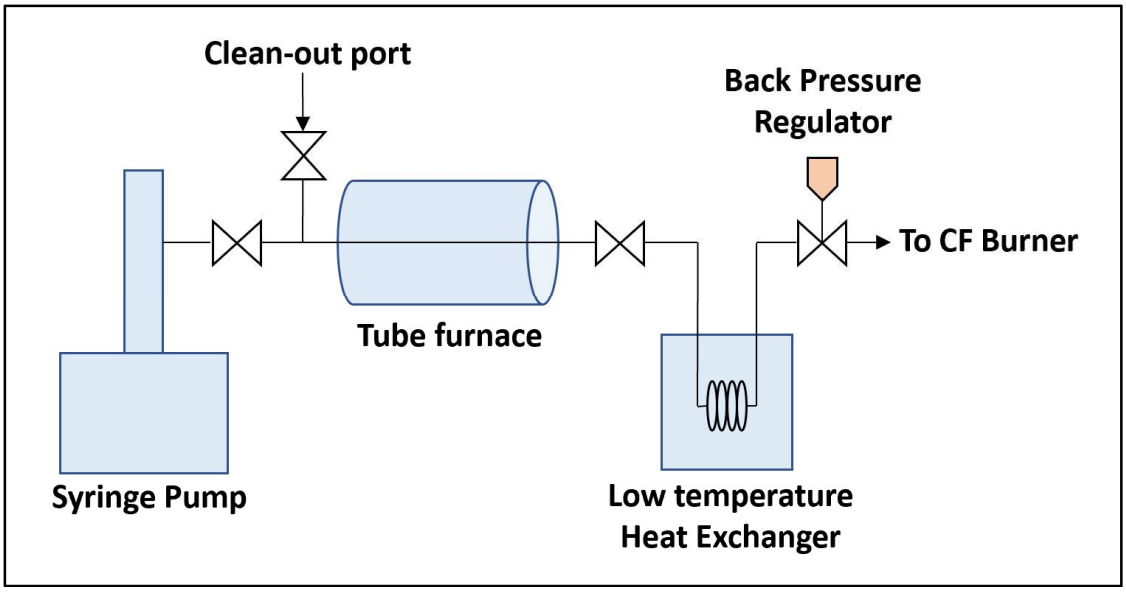

Figure 3.1: High pressure laboratory bench schematic

A total 10 conditions were measured in the flow reactor with varying flow rates for each fuel are described below in the Table 3.1. The temperature of the split tube furnace was kept at 650 °C to get the readings for 600 °C case, and 690 °C for 650 °C case. The overheating of the furnace was done to match the composition of the species that were obtained previously using a previous version of the high-pressure reactor manufactured by NREL.

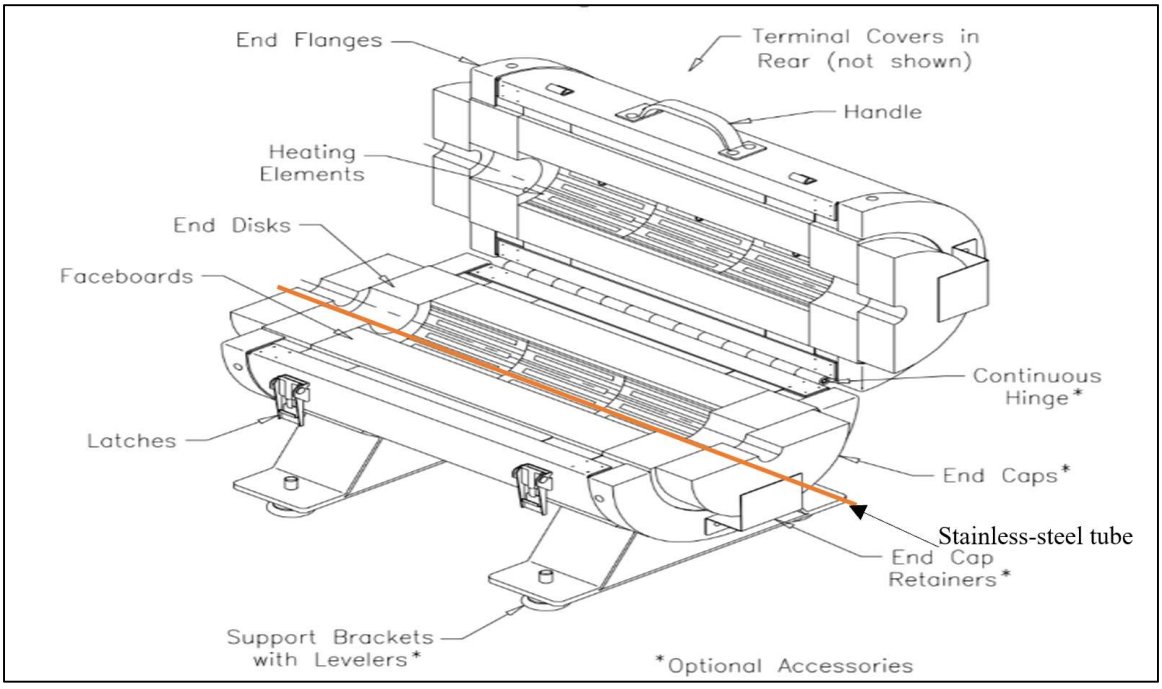

Figure 3.2: Split tube furnace encasing the stainless-steel tube

Table 3.1: A grid showing various pressures and temperatures at which the experiments were carried out

Temperature	600 °C	650 °C
Pressures [atm]	10	-
	50	50
	100	100
	150	150
	170	170

3.2 Burner setup

The measurement of the extinction strain rate was done on the counterflow flame burner. Figure 3.3 shows the schematics of the counter flame flow burner. There are two concentric components for each nozzle assembly. The burner consists of two nozzles of exit diameter 10 mm. The inner nozzle carries fuel and oxidizer for the upper and lower burners respectively. The outer nozzles carry co-flowing N2 that stabilizes the edges of the flames and separates the inner flow from the surrounding atmospheric air. The co-flow diameter is 14 mm. The fuel mixture/oxidizer enters through the main flow passage which is 30 mm in diameter and 85 mm in length. A steel

mesh was used as a flow straightener which combined with carefully designed contours ensures uniform axial velocity profiles at the nozzle exit. This mesh was placed at 30mm upstream the nozzle. The burners have four sets of inlets that delivers the co-flow nitrogen, enabling a shield to the flame from the environment.

This whole burner assembly is mounted on an aluminum frame. The burners are placed in opposing directions. The assembly can be moved horizontally and vertically in order to properly align the burners and to adjust the separation distance. The burners are mounted on the aluminum plates which in turn are mounted on the t-slotted frames via bolts and brackets. The upper burner can move both horizontally and vertically, whereas the lower burner can move only horizontally. A counterflow flame of methane and air was generated to ensure that the burners were concentric. In this project we are using a separation distance of 9 mm between the burners.

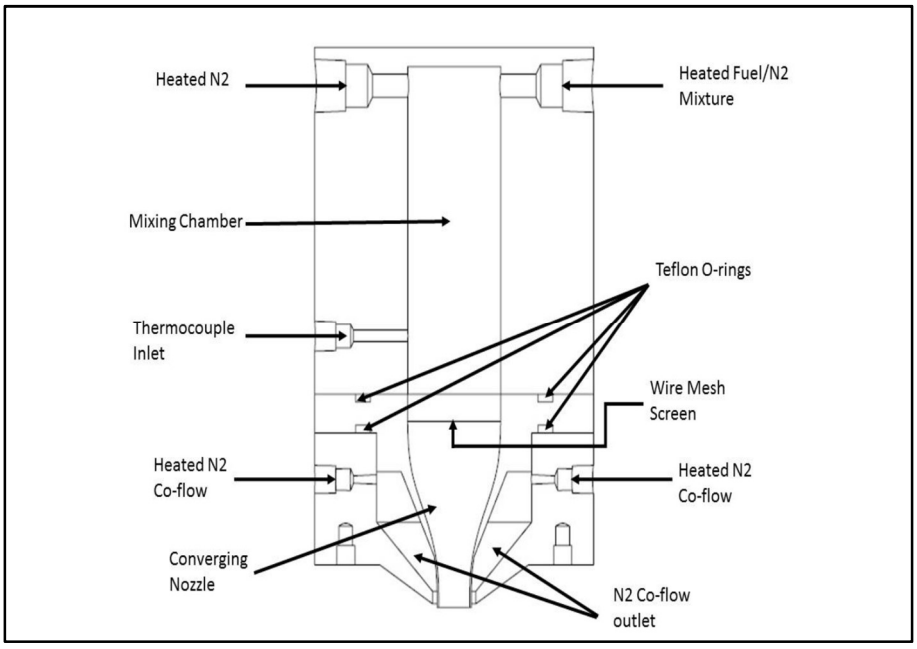

Figure 3.3: Cross section of the fuel delivering burner[41] (Top burner)

Figure 3.4 shows a SOLIDWORKS assembly of the counterflow flame burner assembly. Aluminum t- slotted rails was used as the framing system with two ¼" thick plates. The assembly

dimensions were 18” in height and a width of 12”. Level was used to ensure there is no slant of the aluminum plates.

The volumetric flow rates of the gaseous stream were controlled by using sonic nozzles. By using sonic nozzles, we can monitor the mass flow rate through adjusting the upstream pressure flow. Pressure gauges were installed to monitor the pressure of all gaseous fluids for all experiments.

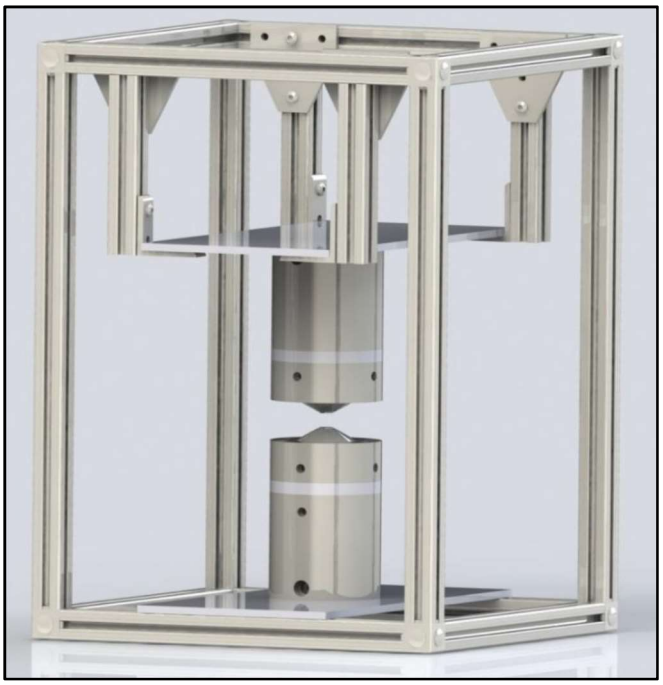

Figure 3.4: SOLIDWORKS assembly[41]

3.3 Fuel vaporization system for liquid fuels

A fuel vaporization system was developed, and its schematic is shown by the Figure 3.5. Fuel enters the vaporizer in a stainless-steel tube of ID 0.016” and is enclosed in another tube which contains heated nitrogen. The ID of this tube is 0.069” and OD of 1/8”. The temperature of the heated nitrogen stream is 100 °C. The fuel and nitrogen stream are combined in a sampling cylinder, which is heated by electrical heating tape. This resulting mixture is vaporized in the

sampling cylinder then directed into the counterflow flame burner in the fuel inlet port identified in Figure 3.5.

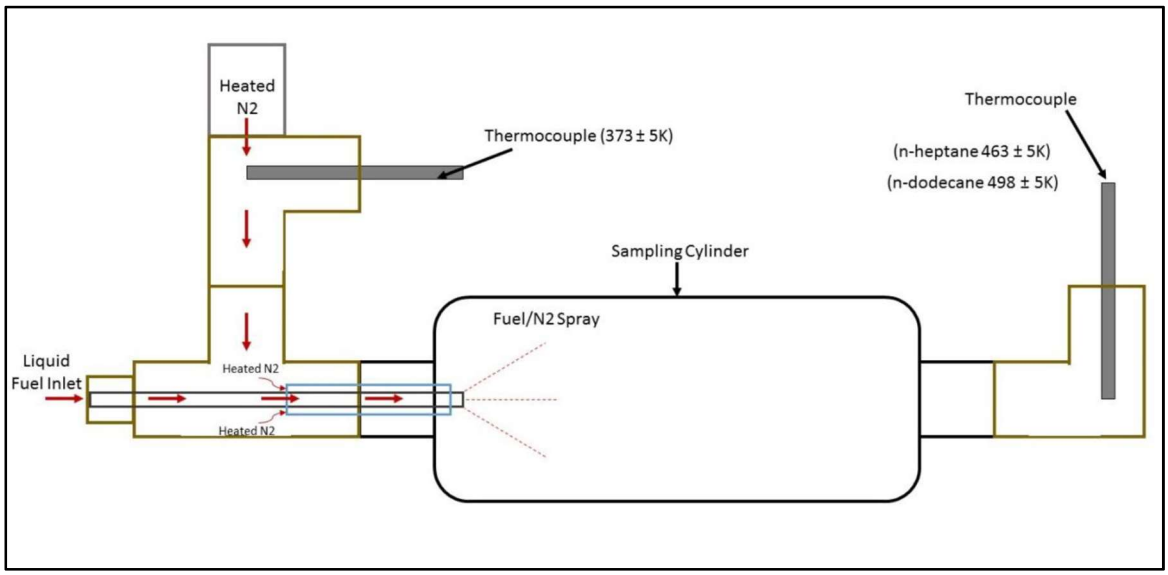

Figure 3.5: Fuel vaporization system[41]

3.4 Flame extinction methodology

To calculate the extinction strain rates, the fuel and air flow rates are increased simultaneously while maintaining a momentum balance, creating a stagnation plane located halfway between the two nozzles, until the flame extinguishes. Once the flame extinguishes, the fuel and oxidizer velocities are noted, and the global strain is calculated by using the equation 2.3. This methodology followed the previous work[42,43,44]. The fuel mass/mole fraction is adjusted, and the experiment is repeated measuring the extinction stain rates for the varying levels of fuel dilution while maintain the momentum balance. The momentum was determined by using the fluid velocity and density of the fuel mixture. The same procedure was followed to calculate the extinction limits of the reacted and unreacted fuel. The experimental data was collected twice to check the consistency of the experiments. The first data set was collected by increasing the flow rate from 0.7 mL/min to 1.5 mL/min, and the second set was taken by decreasing the flow rate

from 1.5 mL/min to 0.7 mL/min. In the result section average extinction strain rated of the fuel is presented.

DIPPR software developed by American Institute of Chemical Engineers is used to find the physical properties of the various species. Properties such as density, enthalpy of combustion are found out. Peng-Robinson method was used to evaluate the density at a given temperature and pressure.

3.5 Setup validation

To validate the experimental setup, methane-air counterflow flame is generated and the results are compared with that in the literature and numerical model. The upper burner carries heated nitrogen and methane flows. This is done by using OMEGA T-type inline heaters. A TEMPCO Duraband model MBH01003 band heater was fixed on the upper burner to minimize the heat loss. The heaters temperatures were monitored by using K type thermocouples and were PID controlled. The temperature of the mixture was kept at about 400 ± 5K. The oxidizer and the co-flow temperatures were kept at ambient condition (298K).

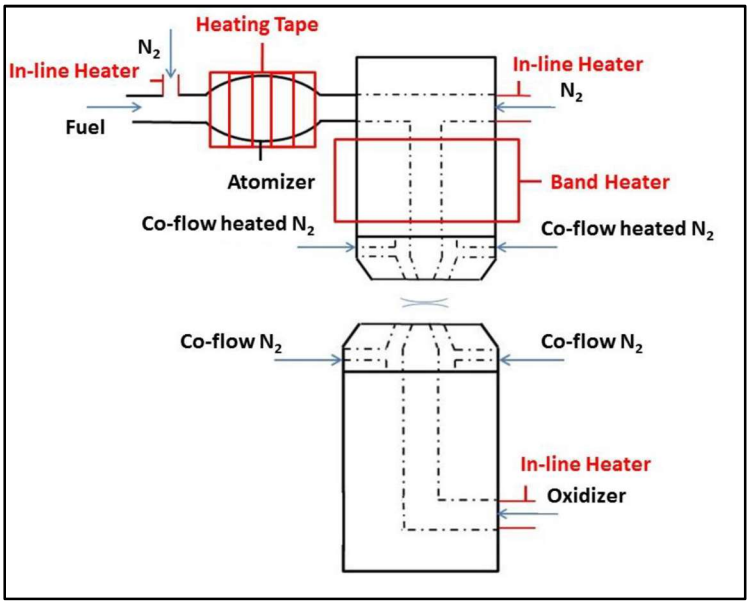

Figure 3.6: Counterflow flame burner configuration[41]

3.6 Sampling of the fuel

The sampling of the fuel was done using Gas Chromatography (GC). The sample was obtained from the nozzle of the upper burner using syringe needle. The needle of the syringe is heated initially to collect the sample, preventing the sample from condensing inside the syringe. The samples are collected at a temperature of 500 ± 10 K, the gas temperature format the exit of the upper burner. The sample is then inserted in the Gas Chromatography/ Flame ionization detector (GC/FID) machine. The highest preheat temperature investigated herein is set to be less than 500 K so that the extent of fuel cracking/pyrolysis within the flow system is considered to be negligible. It should be noted that the sample collection is done before establishing the flame.

An HP 5890 Series II GC/FID was used to analyze the composition of the sample according to ASTM D6729. The identification of species was done by comparing the retention times to those measured with the reference standards. The carrier gas used in the GC was Helium. The following Table 3.2 represents the GC operating condition

Table 3.2: ASTM standard procedure

Chromatographic Conditions	Requirements
Injector settings	
Injector temperature °C	250
Split ratio	175:1 - 275:1
Liner	Deactivated glass
Injection volume, µL	0.2-0.5
Detector settings	
FID detector temperature, °C	300-350
Gas flows	
Hydrogen, mL/min	30-40
Air	300-450
Nitrogen make up, mL/min	30
Column oven settings	
Initial temperature, °C	0
Initial time, min	15
1st ramp rate, °C/min	1
Final temperature, °C	50
Final time, min	0
2nd ramp rate, °C/min	2

Final temperature, °C Final time, min 3rd ramp rate, °C/min Final temperature, °C Final time, min	130 0 4 270 0
Pressure, psig	40-50
Flow, mL/min	1.7-2.0
Linear gas velocity, cm/s	24.5

Chapter 4: NUMERICAL MODELING

For studying the kinetics of reacting systems, especially a steady state steady flow a plug flow reactor is used. Figure 4.1 shows an ideal plug flow reactor assumes no mixing in the axial direction, which means that molecular and/or turbulent mass diffusion is negligible in the direction of the flow. There is a perfect mixing in the direction perpendicular to the flow. It is a frictionless flow that follows the ideal gas behavior. Thus, we can say that the reactor is made up of infinitesimally thin cylindrical plugs of the fluid that flow through the reactor. The plugs have a uniform temperature, axial velocity and species composition at a given location.

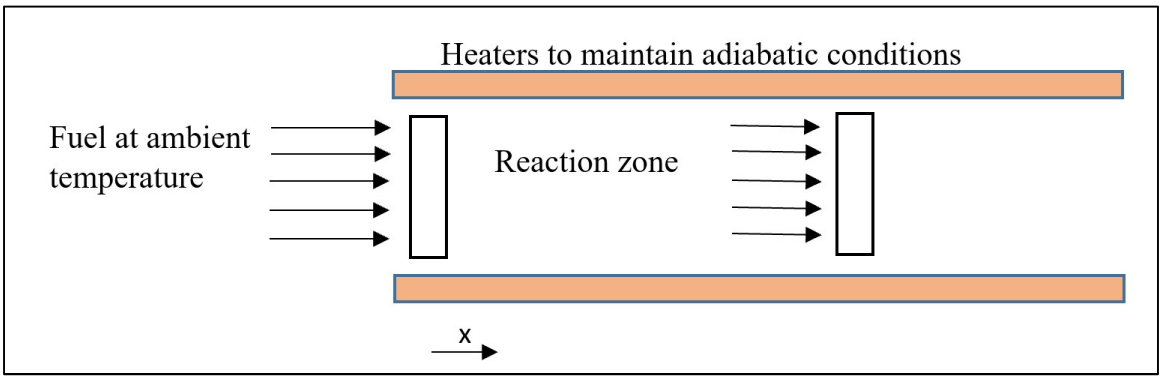

Figure 4.1: Ideal plug flow reactor

The plug flow reactor can be used to study the effect of oxidation and pyrolysis on the fuel. By this we can know the composition of the ensuing species as a function of temperature, pressure and residence time.

4.1 Plug flow reactor modeling

A PLUG[40] module of CHEMKIN was used to simulate the experiments of the thermal decomposition a fuel (n-heptane) can experience. The detailed C8-C16 n-alkanes chemical mechanism obtained from Lawrence Livermore National Laboratory was used in this study[48]. This mechanism has been developed and used to study the pyrolysis and oxidation of nine alkanes larger

than n-heptane also it includes high temperature and low temperature chemistry set. The modeling was compared to the experiments for the pressure ranging from 1 to 80 atm, temperatures from 650 K to 1600 K, equivalence ratios from 0.2 to 1.5 (including pyrolysis). This model was chosen instead of the n-heptane detailed mechanism developed by LLNL[49] because the thermally decomposed n-heptane model exhibited a non-physical trend with pressure, which opposed the experimental results. The C8-C16 n-alkanes mechanism contained 1282 species and 5030 elementary reactions. When the pressure of the reactor was increased the decomposition observed in the fuel was almost constant.

For modeling the reactor, the dimensions were based on the experimental conditions. The inner diameter of the tube was 0.022 inches, the length of the reactor was 25 cm. The temperature for the model were 600 °C and 650 °C and the pressures examined were 13.6 atm, 50 atm, 100 atm, 150 atm and 170 atm. Since the measuring of the extinction strain rates is based on the volumetric flow rates of the fuel the residence for each flow rate case changes. The conditions for the residence time based on the fuel flow rates are given in the Table 4.1:

Table 4.1: Residence time in the reactor according to the volumetric flow rates

Volumetric flow rate [mL/min]	**Residence time[secs]**
0.7	21.02
0.8	18.39
0.9	16.35
1	14.71
1.1	13.37
1.2	12.26
1.3	11.31
1.4	10.51
1.5	9.81

The predicted composition of the fuel following the PLUG[40] simulations subsequently served as the input parameter to the OPPDIF[40] module, required to predict the extinction strain of the decomposed fuel.

4.2 Mechanism Reduction Workbench

CHEMKIN Workbench was used to reduce a master combustion mechanism to a skeletal mechanism. A detailed chemical mechanism of nC8-nC16[48] was used as the master mechanism. A closed homogeneous reactor was used to find the ignition delay. By using this reactor, we are reducing the elementary steps and intermediate species which in turn reduces the required computational capability. The DRGEP method is used for the reduction of the mechanism. The target parameters which are used to compare the reduced mechanism with the master mechanism were ignition delay times, chemical heat release and OH concentration. The species of interest that must be included in the reduced mechanism were selected from the reactor. The final mechanism had 136 species and 852 reactions.

4.3 Counterflow flames

An OPPDIF module of CHEMKIN was used to model the counterflow flames of unreacted n-heptane and n-dodecane and, reacted n-heptane. For n-heptane counterflow flames, a reduced mechanism was generated using the Reaction workbench by using the previous procedure. The mechanism contained 136 species and 852 reactions. The UCSD skeletal chemical mechanism was used for the methane counterflow flame modeling and consisted of 50 species and 235 reactions[50]. For n-dodecane, the LLNL Westbrook reduced mechanism was used which consisted of 106 species and 420 reactions[51]. The composition of fuel mixture was given according to the species present in the reactor after decomposition. For all flow the oxidizer was air, the separation distance between the two nozzles was 9 mm and the pressure and temperature were 0.84 atm and 298 K, respectively. For validation of the counterflow flame burner methane flame simulations were run. And for the n-heptane fuel the fuel stream temperature was 500 K. The numerical simulations were also carried by following a similar procedure to that of the experiments. The velocities of the fuel

and the oxidizer were increased gradually till the extinction was observed[52]. The resulting velocities were the input to the extinction strain rate equation.

Chapter 5: RESULTS AND DISCUSSION

The variable pressure high temperature reactor was used to investigate two reactor temperatures while varying the reactor pressure on the thermal decomposition of the n-heptane fuel. The GC/FID results of the thermally stressed fuel at various reactor pressures and temperatures were analyzed. The results from the experiments are also compared with the numerical modeling from the LLNL higher alkanes detailed kinetic mechanism. The validation of counterflow flame burner is done by comparing the experimental data with the predicted data. The extinction strain rates of the unreacted and reacted fuel are determined and compared with the modeled extinction strain rates.

5.1 Pressurized reactor results

5.1.1 At 600 °C reactor temperature

The composition of the thermally decomposed fuel was determined using the GC/FID for a range of pressure, at constant temperature of 600 °C and a constant volumetric flow rate of 1mL/min of the fuel. The 1mL/min flow rate was chosen as a stable flame could be achieved for every pressure of the reactor for each fuel at this flow rate. At this flow rate the residence time is 14.71 secs, this means that each infinitesimally small plug of fuel experiences an endothermic effect in the reactor for the stipulated period. The smallest species the GC/FID could detect using the ASTM standard method was methane, this means hydrogen was not present in the experimental composition of the reacted fuel. Due to this the hydrogen mass fraction was found using the simulations, which predicted very small concentrations. Hence hydrogen was neglected when quantifying the stressed fuel composition.

The composition of stressed n-heptane was determined using a gas tight syringe needle from the heated nozzle of the counterflow flame burner. The syringe was heated to avoid the condensation in the needle. Also, the nitrogen flow rate was kept constant for each of the sampling (done at various pressures and temperatures), such that there is a consistency in the GC results. The sampled syringe was then inserted in the GC/FID and the ASTM procedure for fuel analysis was followed, given in the Chapter 3. The major species that accounts for more than 0.1% of the total chromatograph area were considered for the experimental results. Table 5.1 shows the composition of the thermally stressed fuel at a reactor temperature of 600 °C, volumetric flow rate of 1mL/min, and pressure of 170 atm. A total of 81 species were observed in the GC chromatograph, and 15 species were observed in the predicted model. Of the 81 species, 21 species were accounting for more than 0.1% of the area.

Chromatograph from the GC/FID analysis of n-heptane for 600 °C, and at 170 atm pressure is shown in Figure 5.1. The lighter species can be seen coming first in the chromatograph. The retention time for some species such as propene, propane, n-butane and n-heptane are 8.53, 9.2, 11.65 and 59.57 mins respectively. Figure 5.2 shows a zoomed chromatograph of stressed n-heptane from 7 to 14 mins.

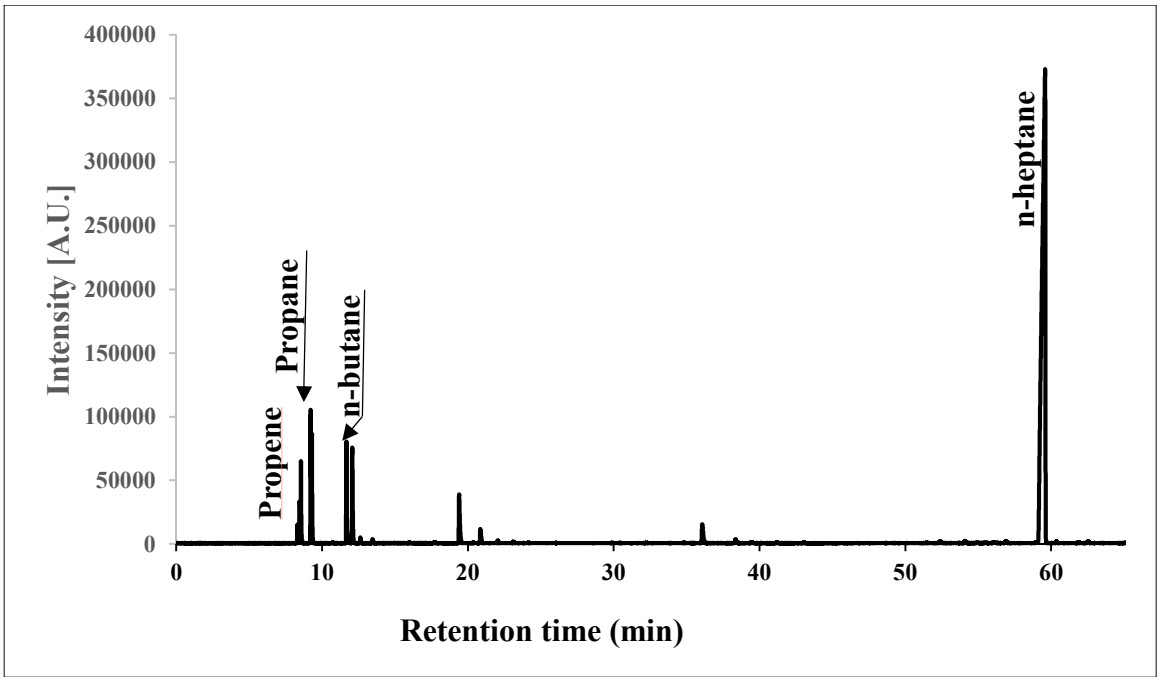

Figure 5.1: GC Chromatograph of stressed n-heptane for 600 °C and 170 atm

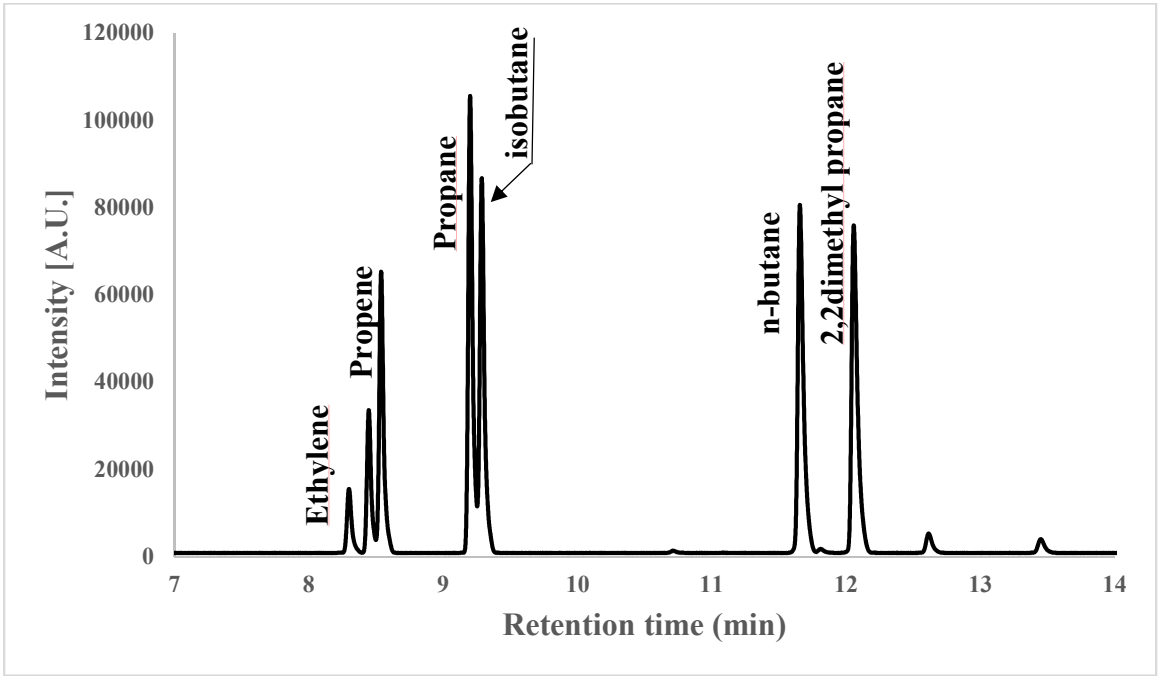

Figure 5.2: GC Chromatograph of stressed n-heptane for 600 °C and 170 atm from 7 to 14 mins

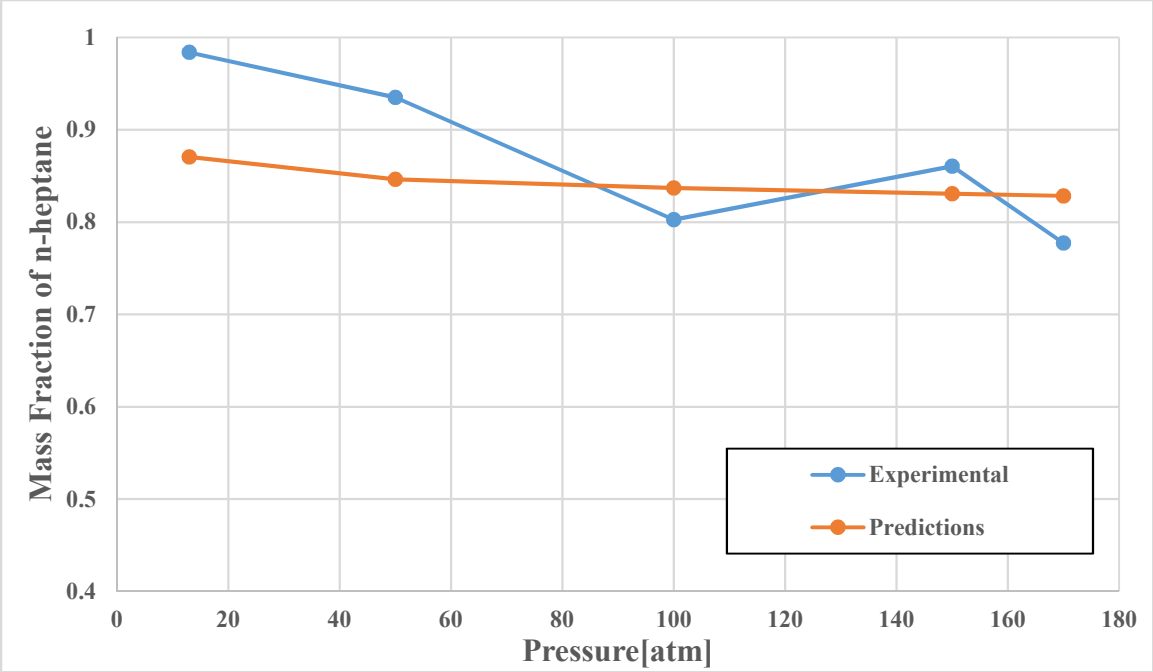

Figure 5.3: Comparison of mass fraction of n-heptane at 1mL/min

Figure 5.3 compares the experimentally determined fuel mass fraction of n-heptane to the predicted modeled plug flow reactor as a function of pressure. Clearly the simulated plug flow reactor over-predicts the thermal decomposition of the fuel for lower pressures i.e. 13.6 atm and 50 atm. This can be attributed to the fact that the simulations of the plug flow reactor were ideal. But in reality, there is a non-ideal behavior in the experiments. The non-ideal behavior such as non-uniformity of temperature along the length of the reactor, wall effects in fuel pyrolysis (Appendix shows the temperature distribution inside the furnace), axial mixing effects, and non-ideal supercritical phenomenon.

The experimental results show more species evolved during the thermal decomposition when compared to the predicted composition. Table 5.1 and 5.2 shows the composition of thermally decomposed n-heptane for the experimental and predicted results respectively. Predictions indicate that there is more production of unsaturated compounds when compared to the experimental results. For example, the production of ethylene in the experiments is 0.48%,

while in the modeling it is 1.5%. Also, experimental results show that there are heavier species formed after n-heptane, but modeling did not show heavier species formation.

Table 5.1: Composition of thermally stressed fuel at 600 °C and 170 atm at 1mL/min flow rate analyzed from GC/FID

Major species	Mass Fraction	Major species	Mass Fraction
Ethylene	0.00485	Cis-2-pentene	0.00127
Ethane	0.00980	1-hexene	0.0118
Propene	0.01992	n-hexane	0.0022
Propane	0.0317	Cyclohexene	0.00131
isobutane	0.028	C7-olefin	0.00136
n-butane	0.031	1-heptene	0.00125
2,2-dimethylpropane	0.0311	n-heptane	0.78531
Cis-2-butene	0.0018	2-methyl-2-hexene	0.00203
3-methyl-1-butene	0.00145	2,3-dimethyl-2-pentene	0.002038
n-pentane	0.0243	3-methylheptane	0.00208
Trans-2-pentene	0.007345		

Table 5.2: Predicted composition of thermally stressed fuel at 600 °C and 170 atm at 1mL/min flow rate

Major species	Mass fraction
Methane	0.007891
Ethylene	0.015586
Ethane	0.027075
Propene	0.025085
Propane	0.002378
1-butene	0.021597
1-pentene	0.029783
n-pentane	0.005969
1-hexene	0.012168
n-hexane	0.013617
1-heptene	0.001238
2-heptene	0.003457
Cis-3-heptene	0.003576
n-heptane	0.828426

In order to account for lack of prediction of decomposition, we have set the temperature of the modeled reactor to match the experimental thermal decomposition of the fuel for each pressure case. This was done to compare the predicted composition with the experimental composition of the reacted fuel. It should be noted that results obtained via this tuning of reactor temperatures are called as shifted results and the predicted results at 600 °C reactor temperature

Table 5.3: Reactor temperatures for shifted data

Pressure [atm]	Modeled reactor temperature [C]
13.6	538
50	563
100	608
150	602
170	613

are called as non-shifted results. The adjusting of temperature of an ideal plug flow reactor has been done previously by varying the initial conditions of the reactor and by changing the boundary conditions[53]. Table 5.3 represents the ideal plug flow reactor temperatures that has been adjusted to match the experimental thermal decomposition of reacted n-heptane at a specific pressure.

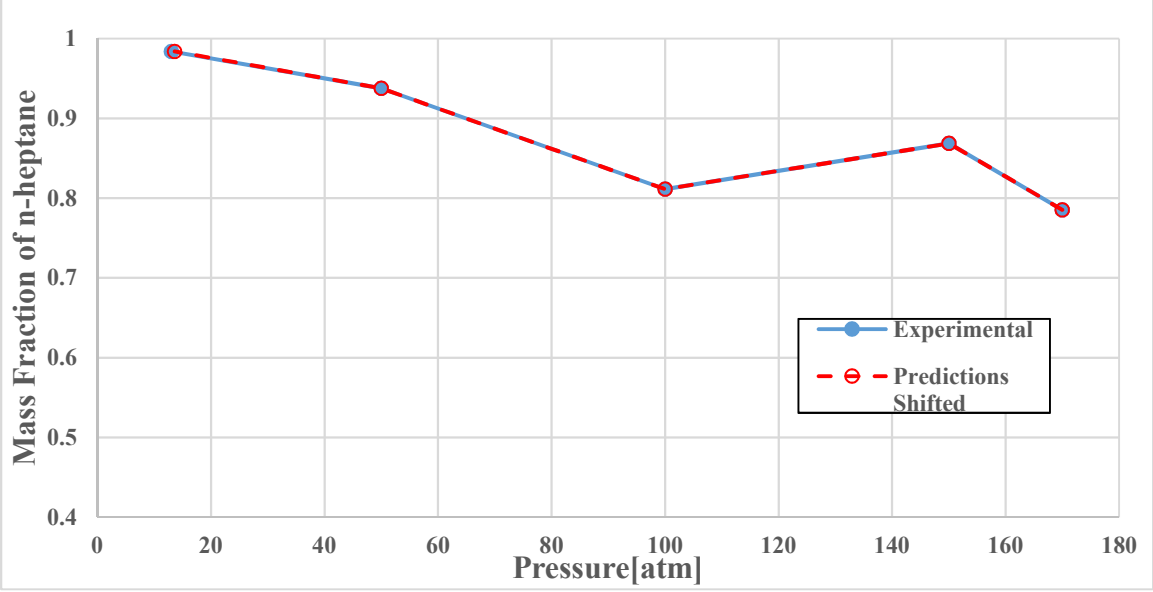

Figure 5.4: Comparison of experimental and predicted shifted mass fraction of n-heptane at 1mL/min

From the Figure 5.4, we can see there is a good agreement between the new predicted mass fractions and experimentally measured mass fractions for each pressure case after tuning the reactor temperature. Also, with the increase in pressure there is an increase in the thermal decomposition of the fuel. At 13.6 atm reactor pressure the mass fraction of the fuel was 0.984, thus there is very little decomposition at this pressure. At 50 atm it was 0.935, at 100 atm the measured mass fraction of n-heptane was 0.802, and at 170 atm the resulting mass fraction was 0.778.

Table 5.4: Composition of shifted thermally stressed fuel at 600 °C and 170 atm at 1mL/min flow rate analyzed from predictions

Major species	**Mass fraction**
Methane	0.009733433
Ethylene	0.01760288
Ethane	0.03289299
Propene	0.03025717
Propane	0.003259633
1-butene	0.02602344
n-butane	0.001120393
1-pentene	0.03695142
n-pentane	0.008360455
1-hexene	0.01519544
n-hexane	0.01788794
1-heptene	0.00176848
2-heptene	0.005048054
Cis-3-heptene	0.005231073
n-heptane	0.7865746

The amount of saturated compounds that are formed during the experiments at 170 atm and 600 °C reactor temperature are about 94.54% and the unsaturated compounds formed make up the remaining 5.46%. For the non-shifted predicted composition, the saturated compounds formed were 88.53% and unsaturated compounds formed were 11.47%. When shifting the reactor temperatures to match the overall n-heptane decomposition, the simulations predicted 85.98% saturated compounds and 14.02% unsaturated compounds. There was more formation of

unsaturated compounds in the shifted predicted composition because the reactor temperature was higher than 600 °C i.e. it was at 613 °C.

It is important to compare the experimental results with the predicted after the temperature shift and check the mass fraction of the species present in the stressed fuel other than n-heptane. Figure 5.4 compares the mass fraction of propene at 600 °C reactor temperature. The experimental results follow the trend of predicted non-shifted results but there is an overprediction of the results by the simulations. At 100 atm and 170 atm the shifted predicted results are overpredicting the mass fraction of propene.

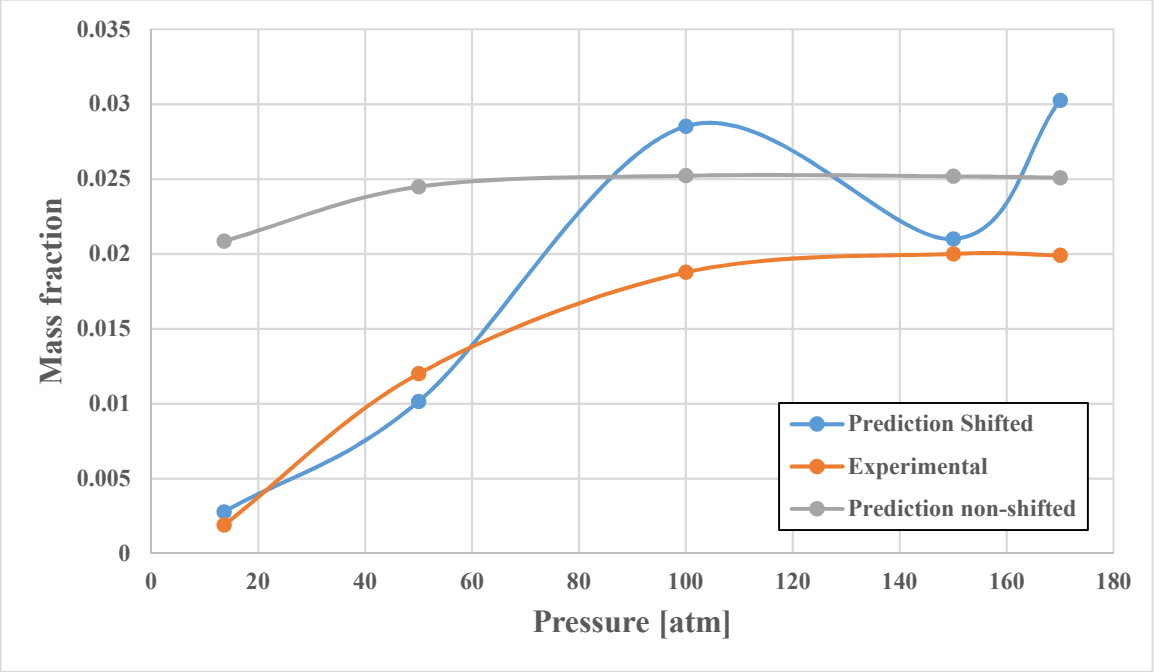

Figure 5.5: Propene formation at various pressures at a reactor temperature of 600 °C

5.1.2 650 °C Reactor Temperature

Similar steps were followed to find the composition of stressed n-heptane at 650 °C. The chromatograph from the GC/FID analysis of n-heptane for 650 °C, and at 170 atm pressure is shown in Figure 5.5. The retention time for some species such as ethyne, propane, n-butane and n-heptane are 8.57, 9.23, 11.69 and 59.48 mins respectively. The number of species observed at 650 °C and 170 atm pressure were 113, and for the predicted model a total of 17 species were observed. Table 5.5 shows the experimental composition of the reacted n-heptane. It should be noted that the predicted modeling had less species because only those species were considered which had a mass fraction more than 0.1%. Of the 113 species, 30 species were accounting for more than 0.1% of the total area.

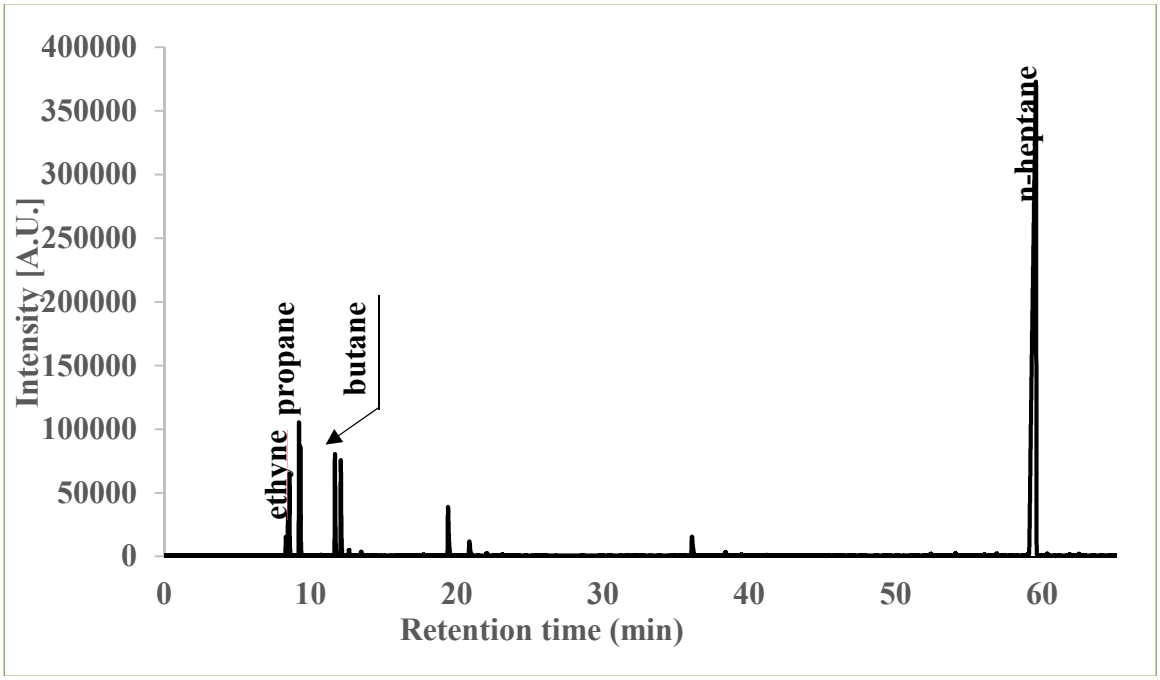

Figure 5.6: Chromatograph of stressed n-heptane for 650 °C and 170 atm

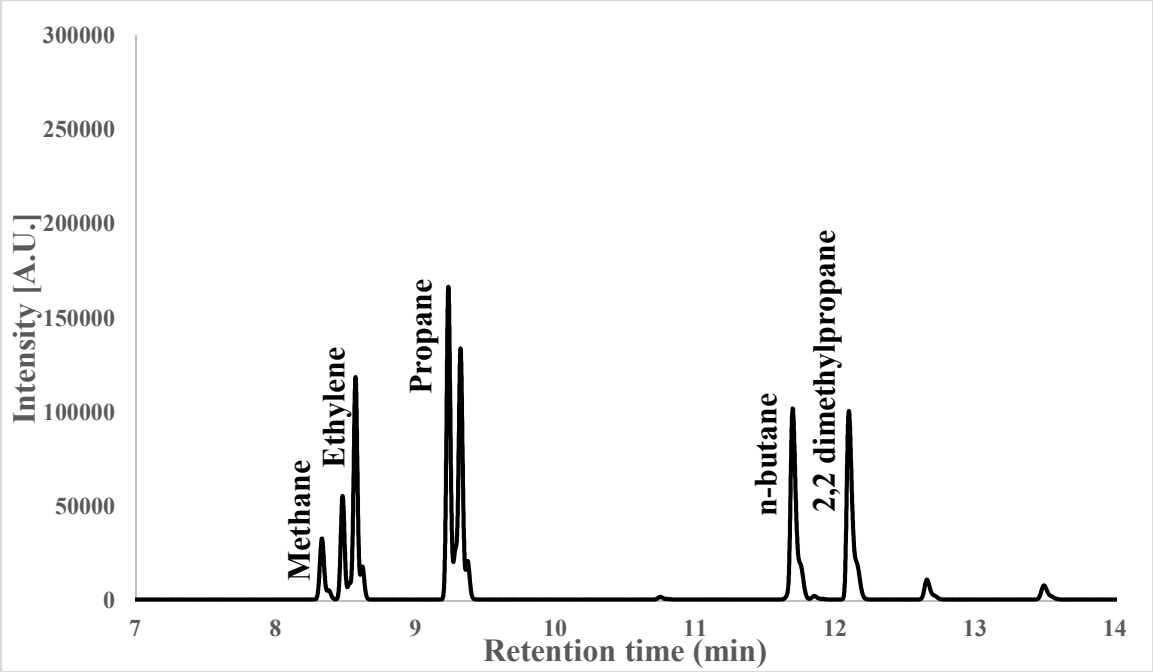

Figure 5.7: GC Chromatograph of stressed n-heptane for 650 °C and 170 atm from 7 to 14 mins

Figure 5.8 compares the mass fraction of n-heptane experimentally measured and predicted as a function of pressure. Similar to the 600 °C case the modeled reactor over predicts the thermal decomposition for the 50 atm, at 100 atm it over predicts the decomposition, and underpredicts the decomposition for 170 atm case. In order to match the experimental results of reactor to the predicted model, the temperatures of the simulations are modified. The input conditions for modeling the reactor were the volumetric flow rates and temperature of the reactor. Previous studies have shown that the composition of the fuel underwent dramatic changes with the increase in temperature[13,14,17].

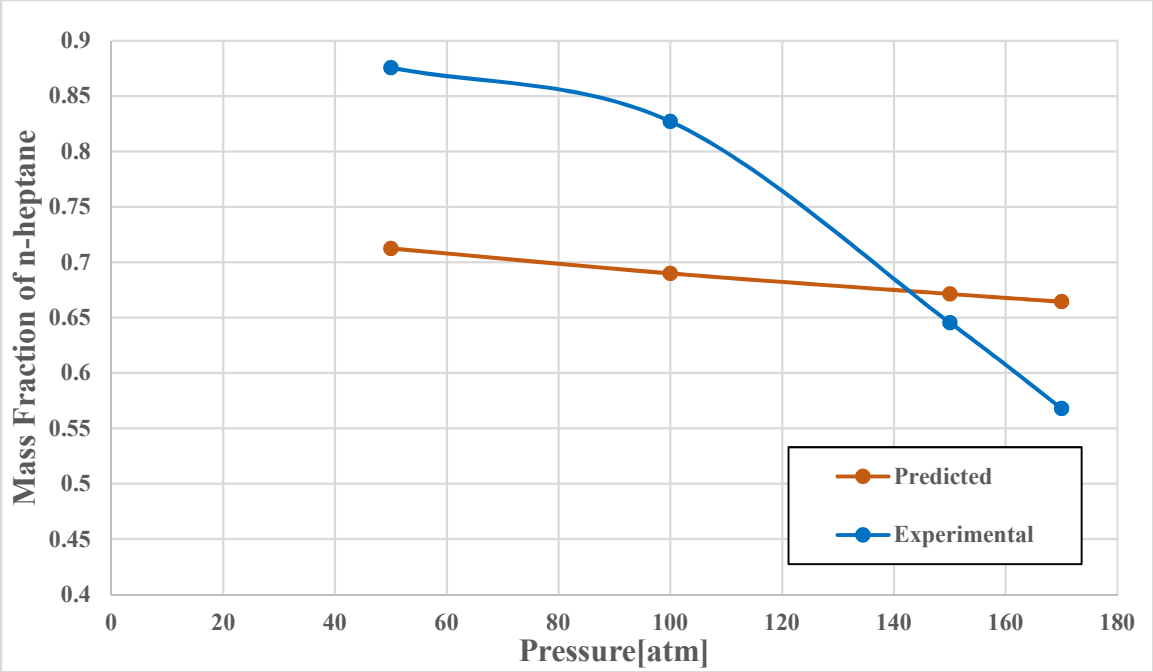

Figure 5.8: Mass fraction comparison of n-heptane at 650 °C

Table 5.5: Composition of thermally stressed fuel at 650 °C and 170 atm at 1mL/min flow rate analyzed from GC/FID

Major species	Mass fraction	Major species	Mass fraction
Methane	0.012824	3-methyl-1,2-butadiene	0.002165
Ethene	0.00149	1-hexene	0.020058
Ethane	0.019898	n-hexane	0.006055
Ethyne	0.044387	trans-3-hexene	0.001827
Propene	0.005592	cis-2-hexene	0.001057
Propane	0.06016	methyl cyclopentane	0.001341
isobutane	0.05646	cyclohexene	0.00139
isobutene	0.006628	c7-olefin	0.001513
butane	0.054355	1-heptene	0.002702
2,2-dimethypropane	0.055312	c7-olefin	0.00134
cis-2-butene	0.006022	n-heptane	0.567864
3-methyl-1-butene	0.004646	2-methyl-2-hexene	0.001835
pentane	0.039652	Trans-2-methyl-3-hexene	0.001035
trans-2-pentene	0.01559	2,3-dimethyl-2-pentene	0.001202
cis-2-pentene	0.003858	3-methylheptane	0.001741

Table 5.6: Composition of thermally stressed fuel at 650 °C and 170 atm at 1 mL/min flow rate analyzed from predictions

Major species	Mass fraction
n-heptane	0.828426
1-pentene	0.029783
Ethane	0.027075
Propene	0.025085
1-butene	0.021597
Ethylene	0.015586
n-hexane	0.013617
1-hexene	0.012168
Methane	0.007891
Pentane	0.005969
Cis-3-heptene	0.003576
2-heptene	0.003457
Propane	0.002378
1-heptene	0.001238

Table 5.7: Reactor temperatures for shifted data

Pressure [atm]	Modeled reactor temperature [C]
50	590
100	605
150	658
170	678

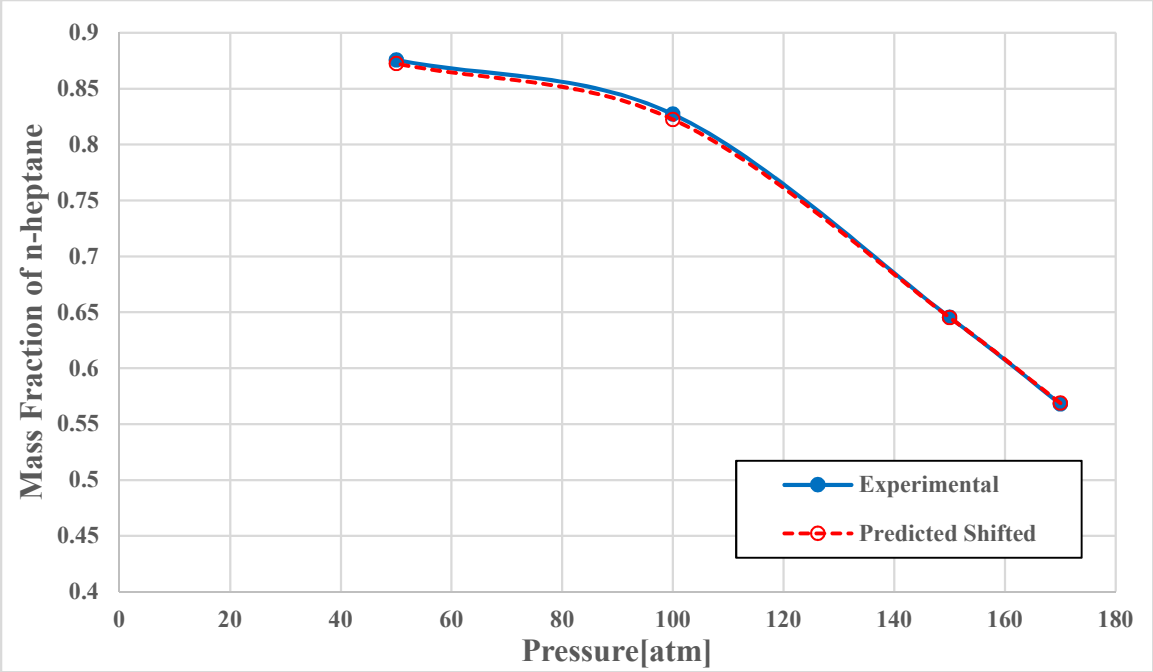

Figure 5.9: Experimental and predicted shifted mass fraction comparison of n-heptane at 650 °C

Figure 5.9 shows the matched mass fractions when the modeled results are modified to match the experimental composition. As the pressure increases the decomposition of the stressed n-heptane fuel increases.

At 50 atm the mass fraction of the decomposed fuel was 0.875, at 100 atm the measured mass fraction was 0.827, and at 170 atm the recorded mass fraction was 0.567. When compared to the 600 C case the values of mass fraction are significantly different. For example, at 150 atm case, the mass fraction for 600 °C is 0.868 and for 650 °C is 0.645. The fuel experiences more decomposition when we increase the temperature of the reactor.

Table 5.8: Composition of shifted thermally stressed fuel at 650 °C and 170 atm at 1 mL/min flow rate analyzed from predictions

Major species	Mass fraction
Methane	0.02023478
Ethylene	0.02086092
Ethane	0.05662295
Propene	0.05079612
Propane	0.008848567

1-butyne	0.001162321
1-butene	0.04294378
n-butane	0.004468586
1-pentene	0.07237236
n-pentane	0.02396642
1-hexene	0.02946782
2-hexene	0.003200272
cis-3-hexene	0.001703986
n-hexane	0.04715484
1-heptene	0.006176518
2-heptene	0.0188308
Cis-3-heptene	0.01962307
n-heptane	0.5687264

The saturated compounds that are formed during the experiments at 170 atm and 650 °C reactor temperature is about 87.56% and the unsaturated compounds forming are 12.44%. For the non-shifted predicted composition, the saturated compounds formed were 78.67% and unsaturated compounds formed were 21.33%. The saturated compounds for shifted predicted results formed were 72.98% and unsaturated compounds formed were 27.02%. There was more formation of unsaturated compounds in the shifted predicted composition because the reactor temperature was higher than 650 °C i.e. it was at 678 °C. When comparing with the experimental 600 °C reactor temperature results the unsaturated compounds are formed more. Thus, we can say with an increase in the reactor temperature there is an increase in the formation of unsaturated compounds.

A similar comparison of a single specie of the experimental results and predicted after temperature shift is done for the stressed fuel. For reactor at 650 °C 1-hexene was chosen to compare the experimental GC results with the predicted one since propene was not formed in some of the experimental cases. There is a good agreement between the predicted and the experimental results shown in Figure 5.8.

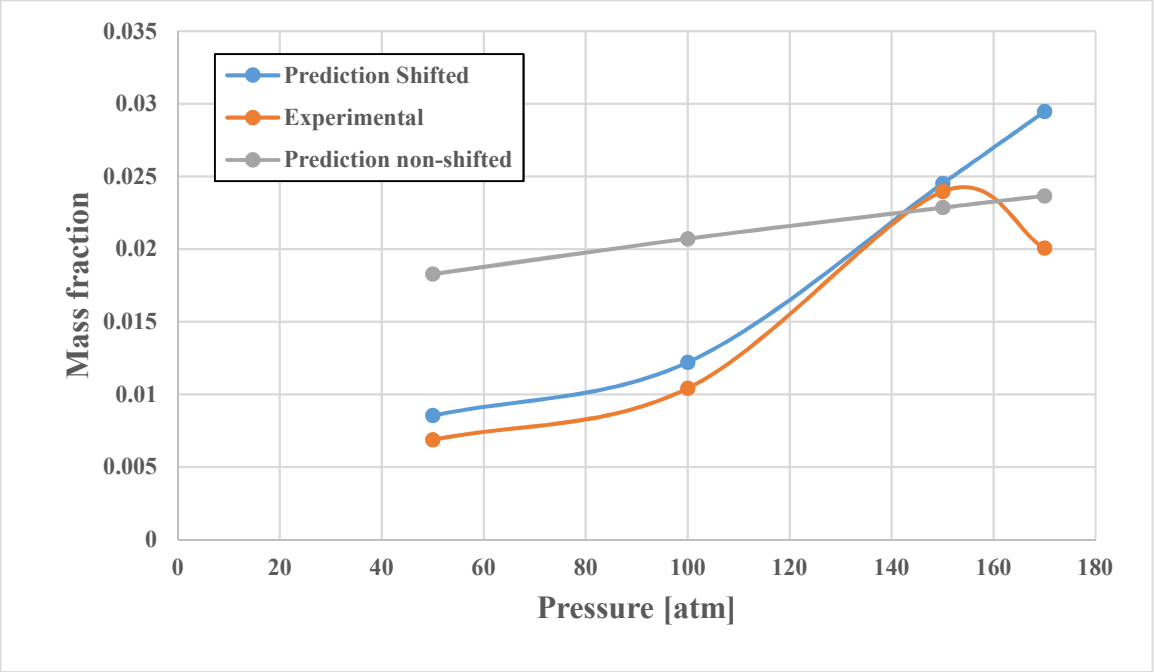

Figure 5.10: 1-hexene formation at various pressures at a reactor temperature of 650 °C

At each pressure and temperature, the molecular weight of the thermally stressed fuel was calculated, and also its density. The density and molecular weight of all the remaining flow rates (i.e. excluding 1 mL/min) for the experimental reactor were calculated using predictions. This was done by scaling the measured experimental results with the predictions. The predicted model provided density and molecular weight for each flow rate. The molecular weight and density are important as they are being used in calculation of extinction strain rates. The molecular weight and density of the fuel decreases as the temperature and pressure of the reactor increases, this can be seen in the next section. For performing the counterflow simulations, the species that made majority of the composition was used.

Figure 5.11 shows the comparison of the thermal decomposition of n-heptane at various pressures and, at 600 °C and 650 °C.

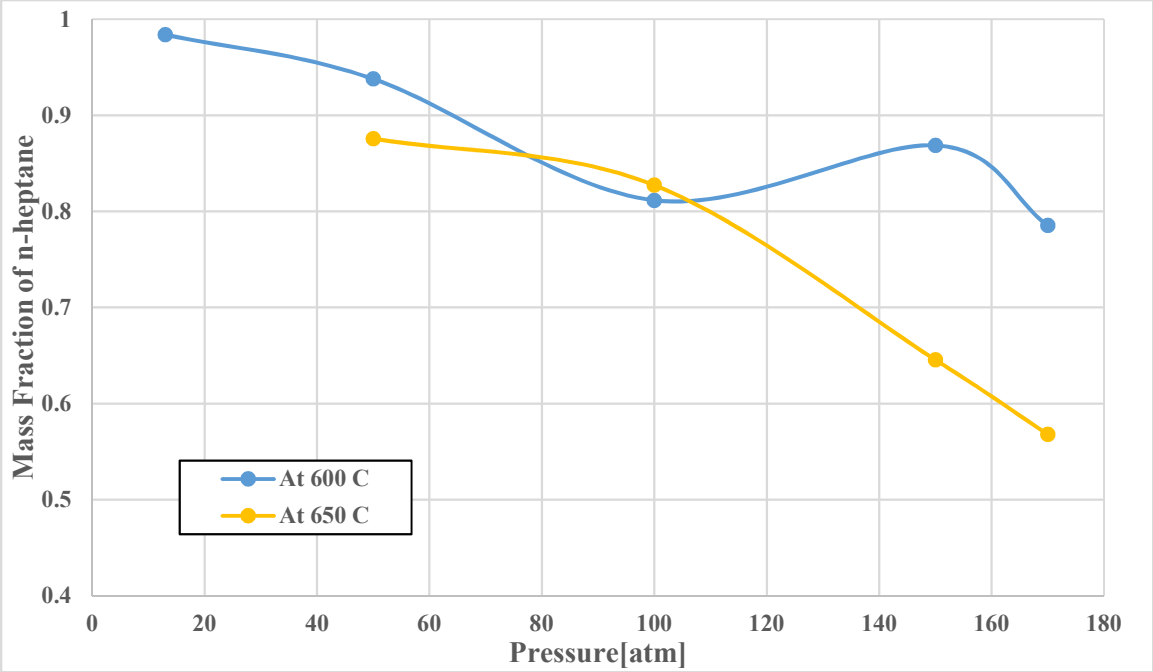

Figure 5.11 Comparison of mass fraction of n-heptane at 600 °C and 650 °C

The thermal decomposition of n-dodecane could not be found because while sampling the reacted n-dodecane the fuel was getting condensed inside the syringe. Due to this, the correct amount of thermal decomposition using GC/FID could not be found out.

To summarize the pressurized reactor results, the non-shifted predicted model using ideal assumptions was not able to effectively predict the amount of thermal decomposition of n-heptane. In order to match the experimental thermal decomposition of n-heptane the temperature of the simulated reactor was adjusted, and the results obtained by this adjustment were called “shifted predicted.” The effect of pressure was seen in the experimental results as higher hydrocarbon species were formed. Even by adjusting the temperature of the modeled reactor, the simulations were not able to predict the composition of the thermally stressed fuel. The thermal decomposition of the fuel increased with an increase in the reactor temperature and pressure. For the results of the non-shifted model, the percent difference of thermal decomposition at 600 °C between the highest and lowest pressures was 4.82% and for experimental results it was 20.11 %. Also, the percent

difference between the highest and lowest pressure at the 650 °C reactor temperature case for the non-shifted model was 6.74 % and for the experimental case it was 35.2%.

The data obtained during the study is unique as there has been no research of thermal decomposition of n-heptane at these high pressures and temperatures of the reactor. The prediction of thermal decomposition by simulations did not accurately predict the experiments at these high temperatures. Also, the shifted predicted composition did not match the experimental composition even when the reactor temperature was adjusted. The reason for this is most likely due to the fact that the chemical kinetic mechanism not being validated at such extreme pressures and that the transport data does not account for the supercritical phenomenon. This data supports the need for additional experimentation and model tuning if wanting to model regenerative cooling.

5.2 Extinction strain rates of unreacted and reacted fuel

5.2.1 Unreacted fuel

Validation of the counterflow flame burner was done using methane as the fuel. The extinction strain rates obtained from the experiments were compared with the numerical predictions as a function of mole fraction and is shown in Figure 5.12. The temperature of the fuel was kept at 400 K and the oxidizer was kept at 298 K. There is a good agreement of the extinction strain rate.

To find the effect of thermal decomposition on flame stability the unstressed fuel's extinction strain rate is measured, and it is then compared with the decomposed fuel. For this unstressed n-heptane extinction strain rate is calculated using the counterflow flame burner. The fuel stream temperature was maintained at 500 K and the oxidizer was kept at ambient temperature of 298 ± 5 K. The fuel was heated and vaporized as described in Chapter 3. Figure 5.13 shows the experimentally measured and simulated extinction strain rate plotted against the unreacted n-heptane mole fraction. The experiments match the trend followed by the simulations, the experimental results are reduced by ~80 s^{-1} when compared with the predictions. This difference can be attributed to the use of reduced chemical kinetic mechanism. From the Figure 5.13 it can be seen that the extinction strain rate increases with the increase in fuel mole fraction. Lastly, we had confidence that our experimental and numerical techniques were measuring the extinction strain rate acceptably and could be applied to different fuel systems.

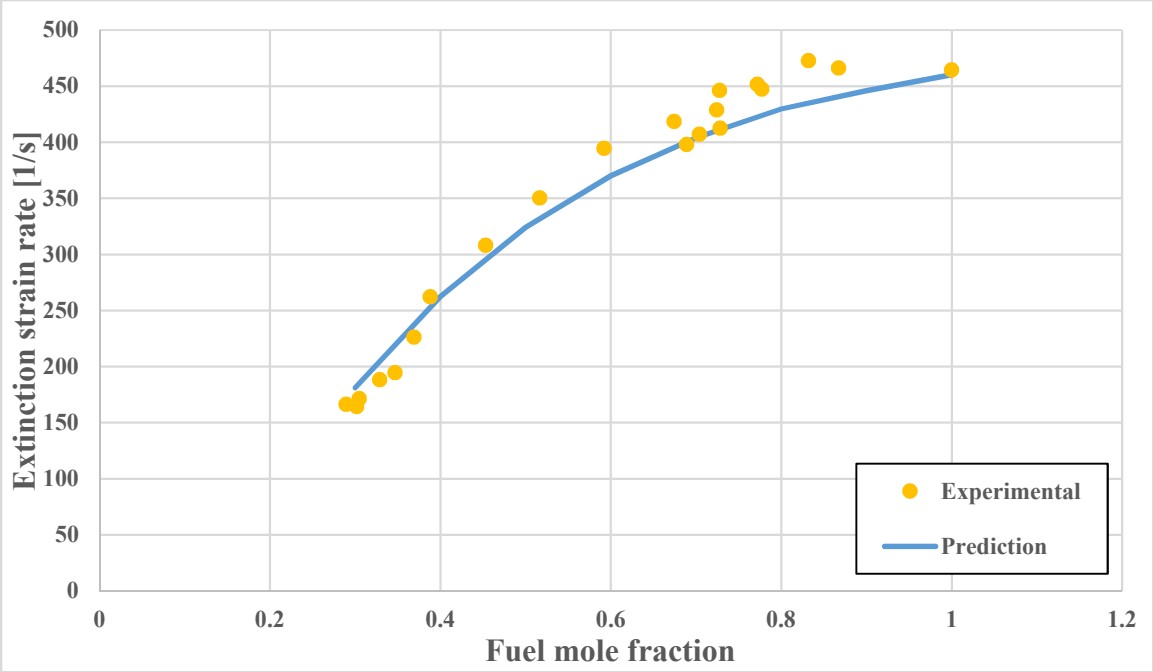

Figure 5.12: Comparison of extinction strain rate of methane

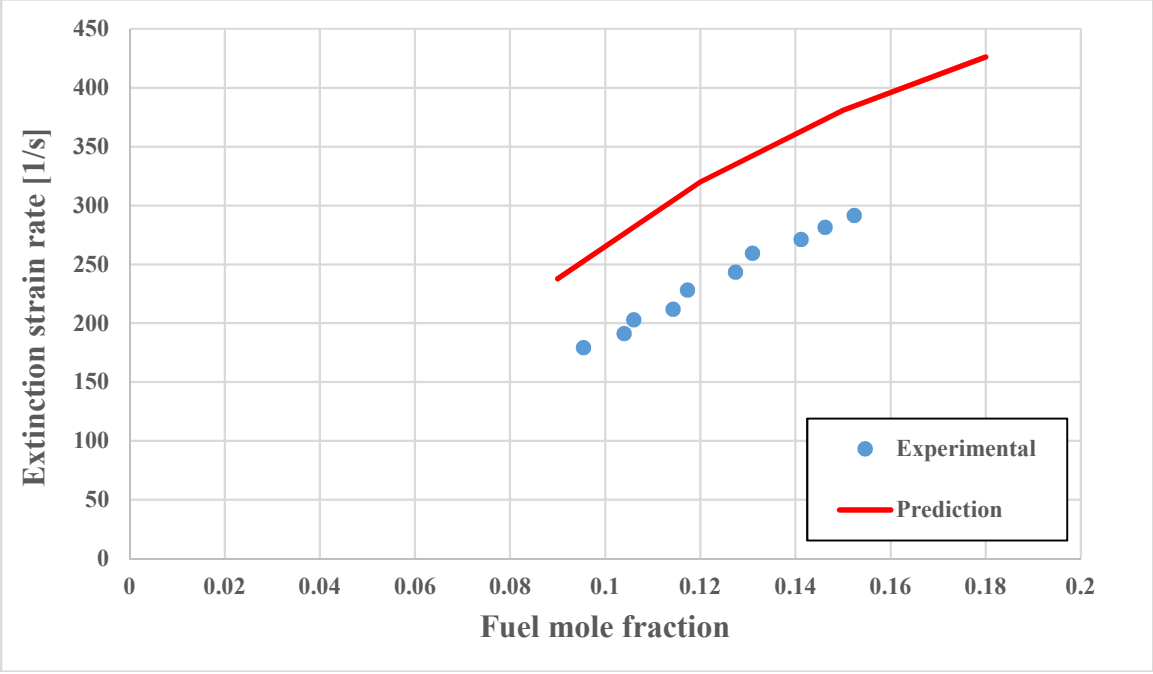

Figure 5.13: Comparison of extinction strain rate of n-heptane

Figure 5.14 shows the extinction strain rate of n-dodecane as a function of fuel mole fraction. It has the same experimental conditions as of n-heptane, the fuel stream was heated to

500 K and oxidizer stream was kept at atmospheric condition i.e. 298 K. The modeled simulation has a good agreement with the experimentally measured extinction strain rate.

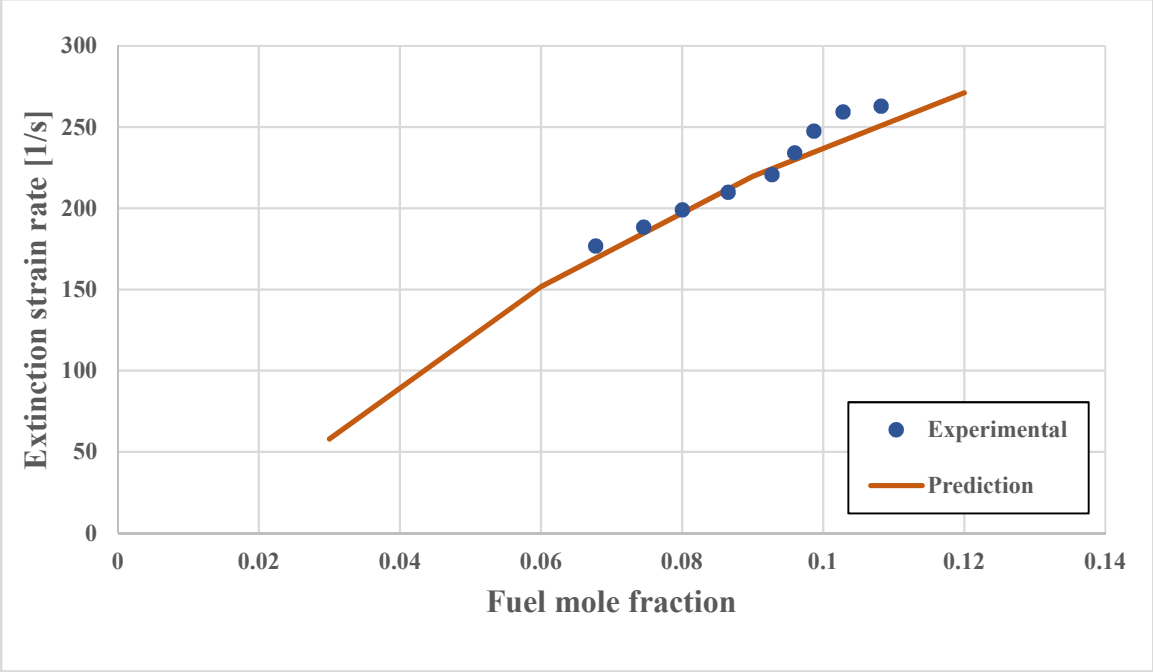

Figure 5.14: Comparison of extinction strain rate of n-dodecane

When comparing the extinction strain rates of n-heptane and n-dodecane it was found that n-dodecane had a higher extinction strain rate than n-heptane shown in Figure 5.15. The difference between the extinction limits of both fuels was about ~55 s^{-1}. The extinction limits vary according to the molecular structure of the fuel, with n-dodecane producing the most robust flame. This trend follows previously reported data and can be attributed to the differences in the chemical kinetics and the molar specific heat of combustion between the two fuels[52].

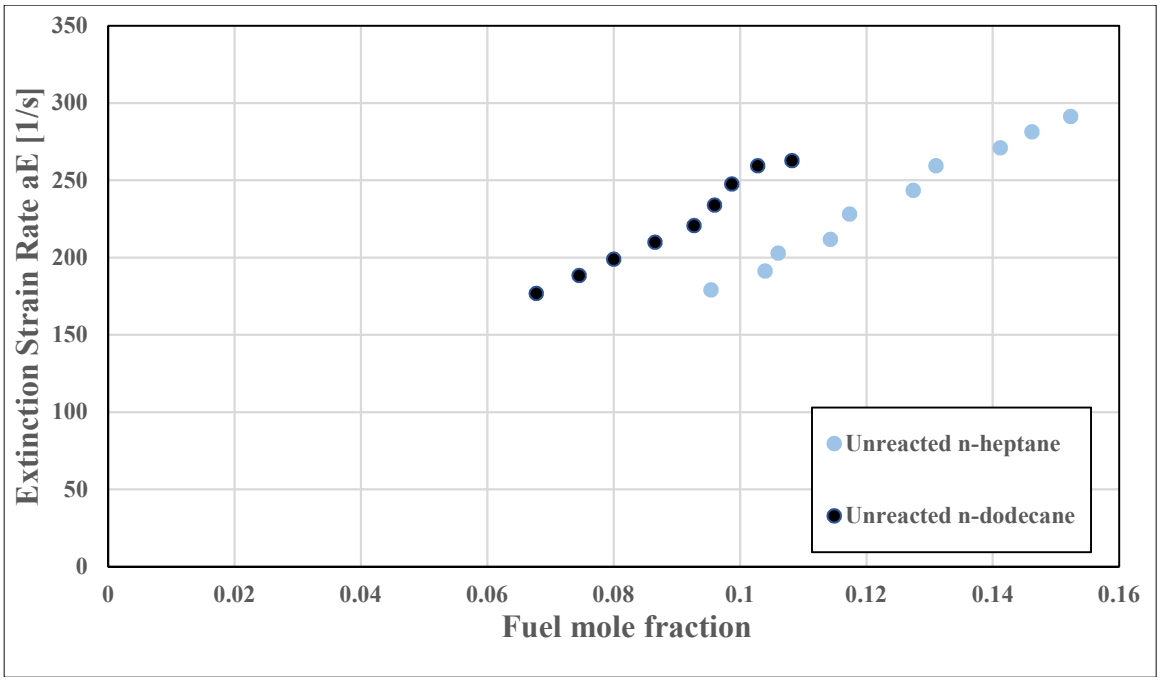

Figure 5.15: Comparison of extinction strain rate of n-heptane and n-dodecane

5.2.2 Reacted n-heptane at 600 °C reactor temperature

The experiments were carried at a reactor temperature of 600 °C with varying pressures. The pressures at which the extinction strain rate was measured were 13.6 atm, 50 atm, 100 atm, 150 atm and 170 atm. The thermally stressed n-heptane from the reactor was fed to the counterflow flame burner. The fuel nozzle temperature was maintained at 500 K for both unreacted and reacted cases, and the oxidizer stream was at 298 K. The molecular weight and density were measured using the results from the GC/FID. The molecular weights and densities for 600 °C, 1mL/min and at various pressures is given in Table 5.9 and 5.10 and were used to calculate the extinction strain rate using equation 2.3.

Table 5.9: Molecular weight of unreacted and reacted n-heptane at given pressure and at 600 °C for flow rate of 1mL/min

Pressure (atm)	**Molecular weight (g/mol)**
Unreacted	100.21
13.6	99.351
50	97.397
100	92.165
150	94.0912
170	91.5327

Table 5.10: Density of unreacted and reacted n-heptane at 0.84 atm and at 500 K for flow rate of 1mL/min (at 600 °C reactor temperature)

Pressure (atm)	**Density (kg/m$^{3)}$**
Unreacted	2.109
13.6	2.075
50	2.0391
100	1.8363
150	1.786
170	1.7184

The molecular weight decreases by about 8.66% for the reacted fuel at 600 and 170 atm. There is also decrease in density of the reacted fuel. Figure 5.16 shows the measured average extinction strain rate against the fuel mole fraction. It can be seen that the extinction strain rate of the fuel increases with the increase in pressure.

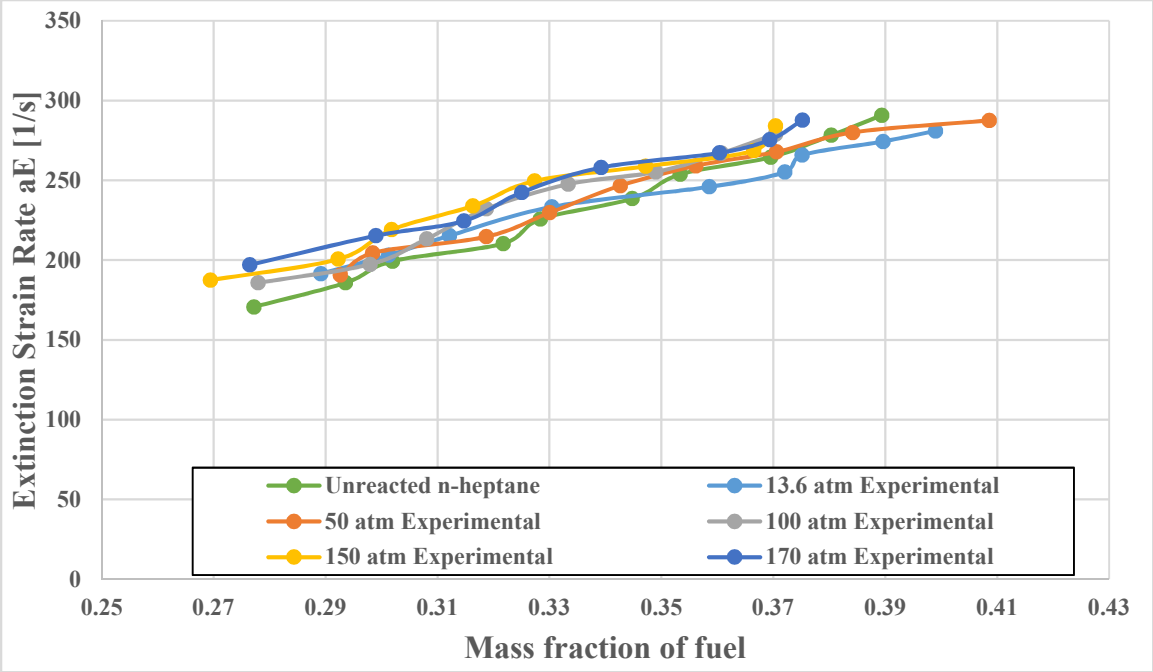

Figure 5.16: Experimental average extinction strain rate of n-heptane plotted against the fuel mass fraction at 600 °C

For a reactor pressure of 13.6 atm the extinction strain rate initially is more than the extinction limits of unreacted n-heptane and then deviates decreasing below the unreacted n-heptane extinction curve with an increase in fuel mass fraction. But a more conclusive result can be seen for the pressures 100 atm and above. At 150 atm and 170 atm the extinction rate is quite the same. This shows that there is an effect of thermal decomposition on the extinction strain rate. The average standard deviation for the experiment was ~4 s^{-1}.

5.2.3 Reacted n-heptane at 650 °C reactor temperature

Similar procedure was followed to calculate the extinction strain rate of stressed fuel at 650 °C. The reactor temperature was set at 650 °C and the extinction strain rate was evaluated at given pressures. It should be noted that the back pressure was not able to produce a pressure of 13.6 atm for 650 C case as it was not able to maintain it. So, for this reactor temperature calculations were done for 50 atm, 100 atm, 150 atm, and 170 atm. The sample was collected using the air-tight syringe and then inserted in GC/FID to get the composition of the stressed fuel. The nozzle end conditions were same i.e. at 500 K. The molecular weights and densities are evaluated at 650 °C, 1mL/min and at various pressure is given in Table 5.11 and 5.12 respectively.

Table 5.11: Molecular weight of unreacted and reacted n-heptane at given pressure and at 650 °C for flow rate of 1mL/min

Pressure (atm)	**Molecular weight (g/mol)**
Unreacted	100.21
50	94.133
100	92.624
150	86.844
170	81.4587

Table 5.12: Density of unreacted and reacted n-heptane at 0.84 atm and at 500 K for flow rate of 1mL/min (at 650 °C reactor temperature)

Pressure (atm)	**Density (kg/m$^{3)}$**
Unreacted	2.109
50	1.812
100	1.751
150	1.566
170	1.341

At 170 atm reactor pressure the molecular weight of the thermally stressed fuel decreases by 18.71 %. Also, the MW decreases by 11.012 % when compared with 600 °C temperature case. The more the heat is absorbed by the fuel the more it breaks down into smaller species. The 650 °C reactor temperature extinction strain rate follow the same trend set by the 600 °C case. But at 150 atm the extinction strain rate is more than the 170 atm for mass fraction above 0.33 shown in

Figure 5.17. Comparing the extinction strain rates at 600 °C and 650 °C, at 0.328 mass fraction for 170 atm reactor pressure shows that there is an increase in extinction strain rate by ~12 s^{-1}. The average standard deviation for the experiment was ~3 s^{-1}.

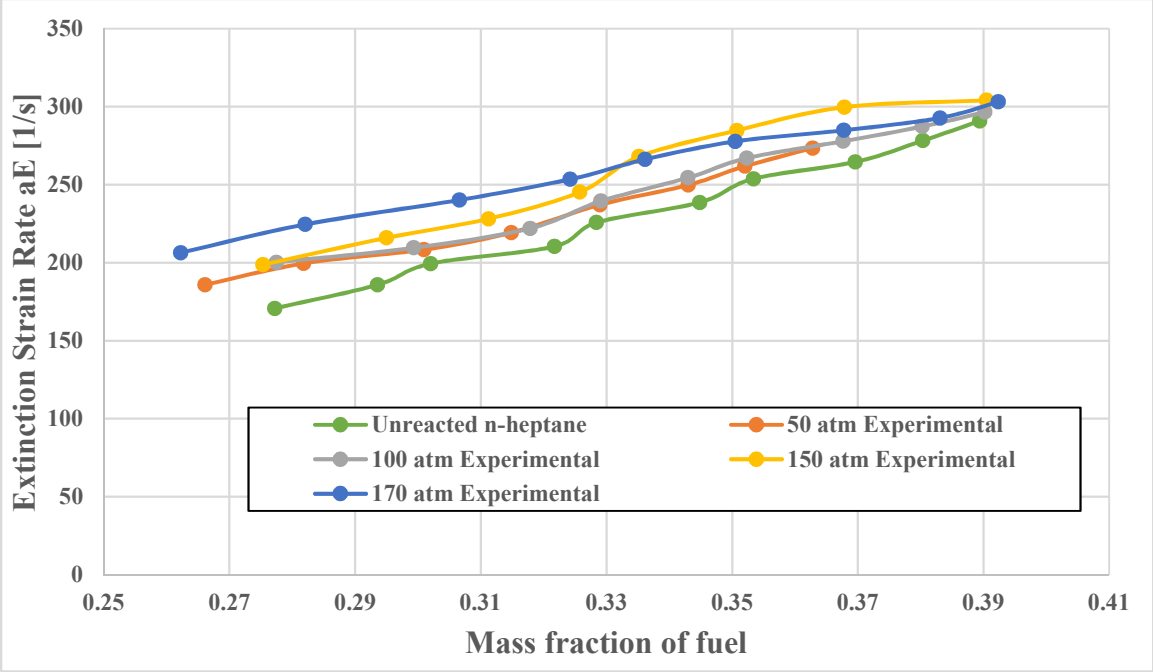

Figure 5.17: Experimental average extinction strain rate of n-heptane plotted against the fuel mass fraction at 650 °C

The numerical computation of extinction strain rate was done using the CHEKMIN. The chemical kinetic mechanism was reduced such that the species that are formed during thermal decomposition are present in the mechanism. It should be noted that a master mechanism was not used for the flame extinction modeling, because it is time consuming. The mechanism was reduced using CHEMKIN workbench, with detailed process described in Chapter number 3. The input conditions were same as the experiments i.e. nozzle exit temperature of fuel stream was kept at 500 K, the oxidizer stream was kept at 298 K. The predicted extinction strain rate of n-heptane is shown in Figure 5.18. This figure depicts the non-shifted numerical predictions. It can be seen that there is a shift in the extinction strain rate of reacted n-heptane fuel at 600 °C reactor temperature

when compared with the unreacted n-heptane fuel. But the extinction strain of reacted n-heptane fuel at various pressures gets overlay on each other. This is because the mass fraction of the predicted thermally stressed n-heptane fuel is relatively similar with varying pressures. Therefore, there is an overlap of the extinction strain rates.

Figure 5.19 shows the predicted extinction strain rate for the shifted numerical predictions. This is done by varying the temperature of the reactor such that it matches the thermal decomposition experienced by n-heptane experimentally.

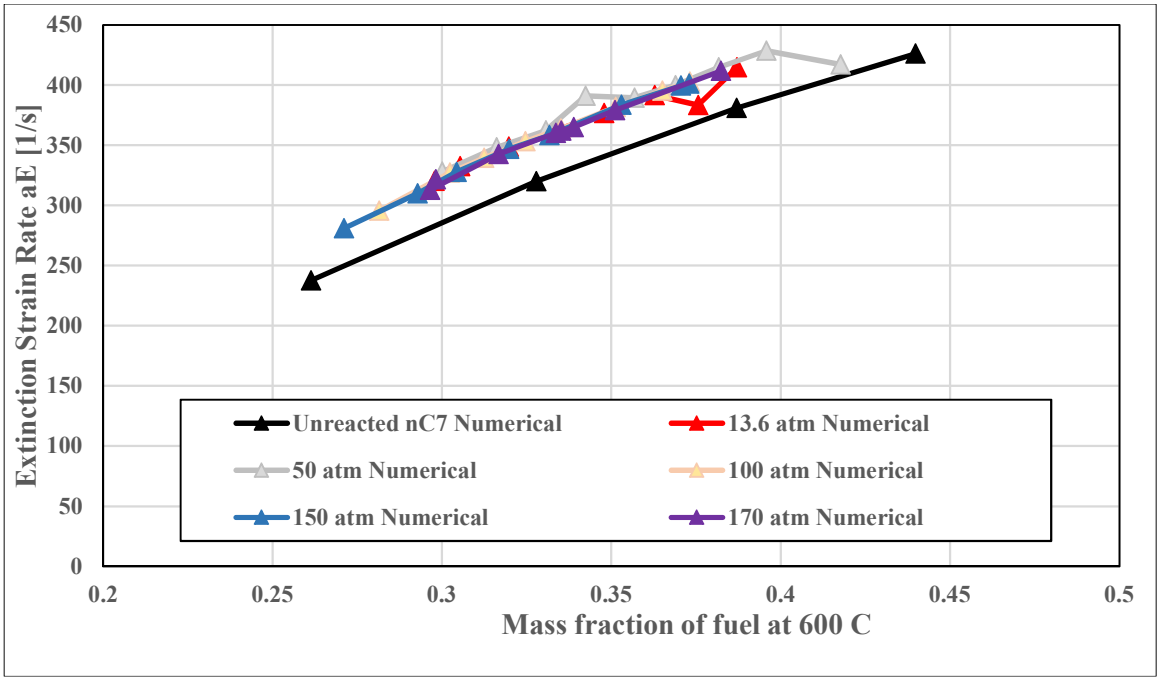

Figure 5.18: Predicted non-shifted numerical extinction strain rate of n-heptane plotted against the fuel mass fraction at 600 °C

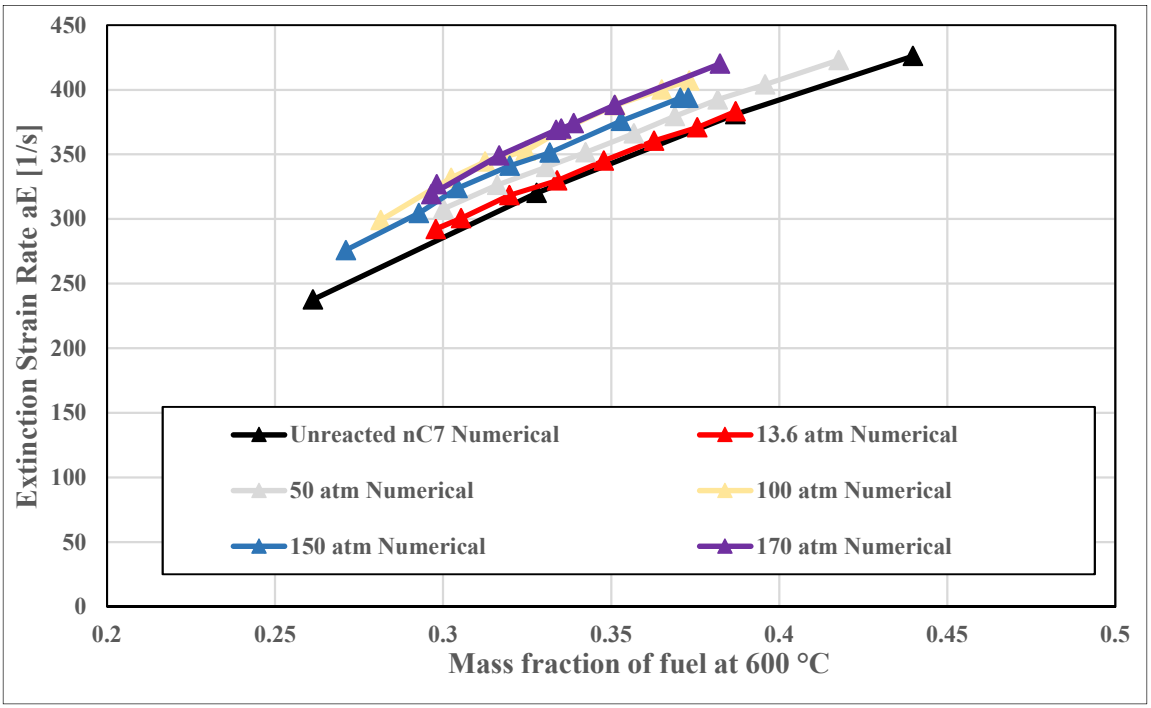

Figure 5.19: Predicted shifted numerical extinction strain rate of n-heptane plotted against the fuel mass fraction at 600 °C

From Figure 5.19 there is much clearer understanding, but for 100 atm reactor pressure the extinction strain rates are quite significant. From the reactor results, 100 atm had a larger percentage of n-heptane decomposed than the 150 atm situation so it affects the extinction strain rate. The trend followed by the experimental results resembles the numerical simulations relatively well.

Figure 5.20 shows the numerically modeled extinction strain rates against the mass fraction of the fuel for the reactor temperature of 650 °C. This is the non-shifted result which means the composition generated by the PLUG reactor is the input to the flame extinction.

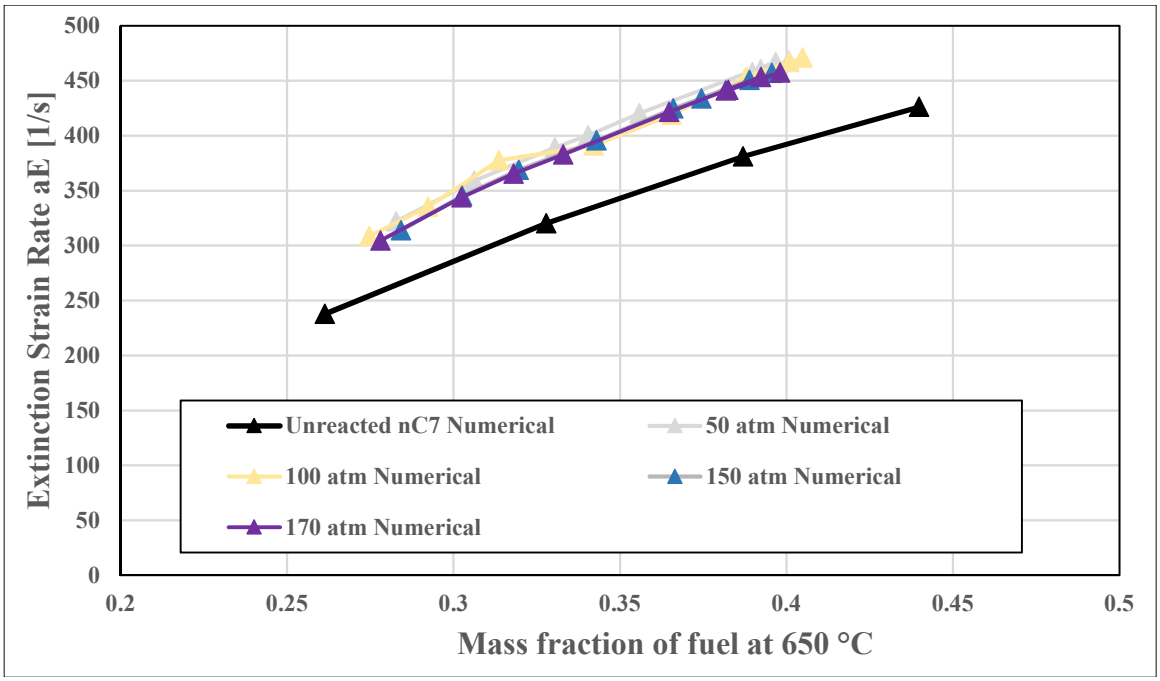

Figure 5.20: Predicted non-shifted numerical extinction strain rate of n-heptane plotted against the fuel mass fraction at 650 °C

Again, like the previous case the extinction strain rates of stressed n-heptane are overlapping on each other. Figure 5.21 shows the shifted predicted extinction rates of n-heptane. In this figure the extinction strain rates are separated and it can be seen that with the increase in pressure the extinction strain rate increases.

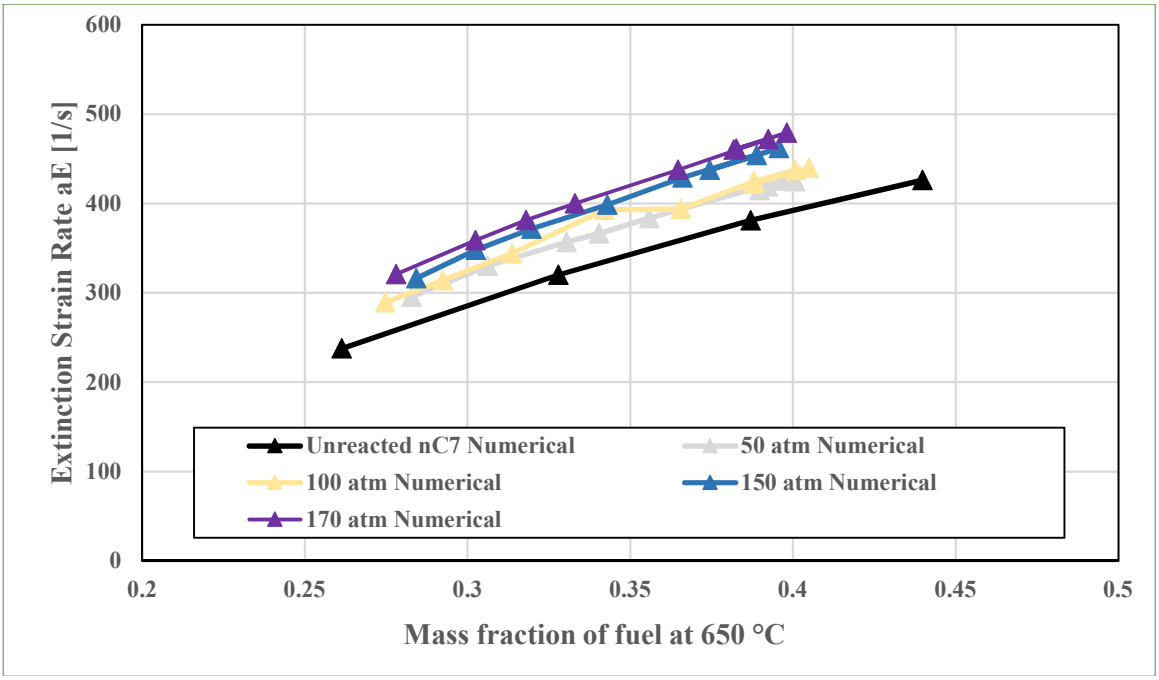

Figure 5.21: Predicted shifted numerical extinction strain rate of n-heptane plotted against the fuel mass fraction at 650 °C

Stressed n-dodecane extinction characteristics could not be measured because the density and molecular weight were unknown.

In summary, the experimental measured extinctions strain rates have a good agreement with the predictions and previous results for methane as a fuel. The simulated extinction strain rate of unreacted n-heptane was overpredicting the experimental extinction limits. The predicted extinction strain rates of the unreacted dodecane agreed well with the experimental extinction limits suggesting that the reason for the poor agreement with the unreacted n-heptane flames is due to the lack of fidelity of the n-heptane chemical mechanism used here. Additional chemical kinetic mechanisms should be investigated. Nevertheless, despite this overprediction in the simulations, the extinction strain rates for the reacted n-heptane did match the experimental trends. The extinction limits of the reacted n-heptane fuel are compared with the unreacted n-heptane, this was done to find out the effect of thermal decomposition on the extinction strain rate. The predicted non-shifted extinction strain rates when plotted against fuel mass fraction showed a minor pressure

dependency. This is because a nominal change in the thermal decomposition of the n-heptane was predicted with the increase in pressure. The experimentally measured extinction strain rates of the stressed n-heptane followed a similar trend to the shifted predicted results both showing a strong pressure dependency where the extinction strain rates of the reacted n-heptane increased with an increase in the pressure

When accounting for errors in the reactor modeling by matching the total n-heptane decomposition, similar trends related to the change in flame stability were noticed between the predictions and experiments with an increase of flame extinction strain rates as reactor pressure increased. These trends were observed at both reactor temperatures of 600 °C and 650 °C. A further increase in extinction strain rate was noticed when the reactor was operated at higher temperatures. Thus, it can be inferred that more thermal decomposition leads to a more stable flame. Previous work presented by Won et al.[52] investigated the thermal and mass transport effects that were resulting from the chemical kinetics which lead to the extinction of diffusion flames for larger hydrocarbon fuels. Won concluded that the extinction strain rates of diffusion flames are proportional to the enthalpy of combustion and rate of mass transport of fuel, represented by the molecular weight. According to the author the extinction strain rate will be higher for a fuel that has a larger enthalpy of combustion, a smaller molecular weight and the ability of the fuel to produce more active radicals. Increased formation of more unsaturated species (which possess greater enthalpies of combustion than the corresponding saturated hydrocarbon) occur at higher pressures and temperatures and the molecular weight of the reacted fuel is also minimized. As a result, this means we can realize a more stable diffusion flame. Given that the counterflow flame predictions showed similar trends, the reactor modeling appears to be the weak link in predicting the experiment. Additional efforts should focus on this aspect. However, additional flame studies

are needed to understand why the n-heptane predictions in general over predict the experimental data.

Chapter 6: CONCLUSIONS

This study investigated the effect of thermal decomposition on the extinction strain rate of n-heptane fuel using high pressure reactor at two reactor temperatures of 600 C and 650 C, and for pressures ranging from 10-170 atm. The ultimate goal was to explain how changes in thermophysical properties (e.g. molecular weight, heat of combustion, etc.) due to endothermic reactions of thermally stressed fuel affected the extinction strain rates of a hydrocarbon fuel. Following are the conclusions from this study:

1. Validation of a counterflow flame burner was done using common gaseous fuels (methane) by comparing the numerically modeled extinction strain rate. There was a good agreement between the experimental and predicted data which infers that the counterflow flame burner was effective method to be used for measuring the extinction strain rate of the thermally stressed fuels.
2. The simulated results obtained from CHEMKIN underpredicted the decomposition of n-heptane at both reactor temperatures of 600 °C and 650 °C for higher reactor pressures, and overpredicted the decomposition for lower reactor pressures. To correct for non-idealities in the measurements, and obtain predicted compositions that better match the measurements, the temperature for each reactor pressure was calibrated such that the resulting mole fraction of n-heptane. Even after matching the total fuel decomposition, for both the reactor temperatures of 600 °C and 650 °C, the composition of the stressed fuel did not predict that of the experimental data, nevertheless, the trend observed was similar to the experimental data for the thermal decomposition i.e. the fuel decomposed more with increase in temperature and pressure.

3. More decomposition of the fuel was observed as the reactor pressure and temperature increased. More species were formed with an increase in reactor pressure and temperature observed in both the experimental results and the modeled reacted fuel composition. The molecular weight and density of the stressed fuel also decreased as the conditions were driven to higher pressures and temperatures.
4. Counterflow flame extinction strain rates increased as the pressure and temperature of the reactor increased (or as the thermal decomposition increased). The predicted extinction strain rate values were very similar when using the predicted composition while considering the thermal decomposition experienced by the fuel while keeping the reactor at a constant temperature for various pressures (i.e. not correcting the predicted composition to match that of the experiments). Using the composition predicted after adjusting the reactor temperatures to match the experimental thermal decomposition, differences in the predicted extinction strain rates were observed and followed similar trends experienced in the measured values.
5. The predicted extinction strain rates in general over predicted the experimentally measured values this may be due to formation of more unsaturated species in simulations when compared to experiments.

6.1 Future work

Moving forward, there are a number of aspects related to the measurements and additional analysis that could be carried out to explain the differences observed between the measurements and the predictions. Performing a sensitivity analysis on the kinetic calculations would aid in the determination the reaction pathways and chemical transport that lead to the predicted results. An improved method to sample the stressed fuel by directly connecting GC/FID to the counterflow flame burner nozzle would improve the measured composition uncertainty. Development of a universal extinction strain rate correlation which includes the effect of pressure would greatly reduce the amount of computation time required to predict flame extinction phenomenon. These alternative approaches would need to be able to account for chemical kinetic differences in the fuels. If this could be done with 0 D reactor simulations, this would allow for the use of detailed kinetic mechanism and eliminate additional error in the calculations when a mechanism is reduced. Carrying out similar approaches using larger fuel structures with differing chemical structures would provide an understanding on how different fuel structures impact the thermal decomposition. It is expected that larger hydrocarbons would experience more thermal decomposition due to their reduced bond energies, and thus a more significant difference in flame extinction would be observed following their decomposition. Real propulsion fuels (e.g. Jet-A, JP-8, etc.) should be studied to inform surrogate fuel selections that can best emulate both the fuel thermal decomposition and subsequent combustion phenomenon.

Statistical investigation including a sensitivity analysis should be done, which will give a better insight of the underlying processes responsible for the poor agreement between the high-pressure reactor predictions and the experimental measurements. The parameters that should be studied may include rate constants, activation energies, thermodynamic constants, and transport

coefficients, especially given supercritical phenomenon. Results from this type of study would support the development of chemical mechanisms identifying what parameters should be first tailored to match extreme pressure reactor data. In addition, experiments should be repeated so that statistical significance of the data and its comparison to predictions can be quantified.

References

1. Huzel, D., K., Huang, D., H., "*Modern Engineering for Design Liquid-Propellant Rocket Engines*", AIAA,1992.
2. Zucrow, M., J., Hoffman, J., D., "*Gas Dynamics: Multidimensional Flows*", vol. 1 & 2, John Wiley & Sons Inc., 1977.
3. H. M. Roder, R. D. McCarty, and W. J. Hall., *"Computer programs for thermodynamic and transport properties of hydrogen*". Technical Report NBS-9288, 1967.
4. Mustafa Emre Boysan- "Analysis of Regenerative Cooling In Liquid Propellant Rocket Engines". Master's Thesis, 2008
5. L. E. Faith, G. H. Ackennan, And H. T. Henderson., "*Heat Sink Capability of Jet A Fuel: Heat Transfer and Coking Studies*"
6. François Falempin., "*Propulsion Systems for Hypersonic Flight*"
7. Seader, J.D., and Wagner, W.R., 'Regenerative Coding of Rocket Engines,' Chemical Engineering Progress Symposium Series, Vol. 60, No. 52,1964, pp. 130-150.
8. Thompson, R. J., 'Investigation of Cooling Problems at High Chamber Pressures,' Rocketdyne, R-3999, May 1963
9. Sutton, G. P., and Biblarz, O., Rocket Propulsion Eiements, 7" ed., Wiley Interscience, New York 2001
10. Yu, G., Li, J. G., Zhao, Z., Chang, X. Y., and Sung, C. J., "Investigation of Vaporized Kerosene Injection in a Supersonic Model Combustor," *American Institute of Aeronautics and Astronautics*, AIAA-2003-6938, 2003.

11. Fanxu Meng, Guozhu Liu, Shudong Qu, Li Wang, Xiangwen Zhang, and Zhentao Mi., “Catalytic Cracking and Coking of Supercritical n-Dodecane in Microchannel Coated with HZSM-5 Zeolites” *Industrial & Engineering Chemistry Research* 2010 *49* (19), 8977-8983.
12. Nacke, Robert, Brittany Northcutt, and Issam Mudawar. "Theory and experimental validation of cross-flow micro-channel heat exchanger module with reference to high Mach aircraft gas turbine engines." *International Journal of Heat and Mass Transfer* 54.5-6 (2011): 1224-1235.
13. Jiang, Rongpei, Guozhu Liu, and Xiangwen Zhang. "Thermal cracking of hydrocarbon aviation fuels in regenerative cooling microchannels." *Energy & Fuels* 27.5 (2013): 2563-2577.
14. Jia, Zhenjian, et al. "Experimental and modeling investigation of n-decane pyrolysis at supercritical pressures." *Energy & Fuels* 28.9 (2014): 6019-6028.
15. Jiao, Si, et al. "Investigation of Pressure Effect on Thermal Cracking of n-Decane at Supercritical Pressures." *Energy & Fuels* 32.3 (2018): 4040-4048.
16. Outcalt, Stephanie L., and Arno Laesecke. "Measurements of density and speed of sound of JP-10 and a comparison to rocket propellants and jet fuels." *Energy & fuels* 25.3 (2011): 1132-1139.
17. Windom, Bret C., and Thomas J. Bruno. "Assessment of the composition and distillation properties of thermally stressed RP-1 and RP-2: application to fuel regenerative cooling." *Energy & Fuels* 25.11 (2011): 5200-5214.
18. Pant, Kamal K., and Deepak Kunzru. "Pyrolysis of n-heptane: kinetics and modeling." *Journal of analytical and applied pyrolysis* 36.2 (1996): 103-120.

19. Garner, S., Sivaramakrishnan, R., & Brezinsky, K. (2009). The high-pressure pyrolysis of saturated and unsaturated C_7 hydrocarbons. *Proceedings of the Combustion Institute*, *32 I*, 461-467. DOI: 10.1016/j.proci.2008.06.217
20. Fridlyand, Aleksandr, Kenneth Brezinsky, and Andrew Mandelbaum. "N-Heptane Pyrolysis and Oxidation in Ethylene–Methane and Iso-Octane Mixtures." *Journal of Propulsion and Power* 29.3 (2013): 732-743.
21. Potter, A. E., and James N. Butler. "A novel combustion measurement based on the extinguishment of diffusion flames." *ARS JOURNAL* 29.1 (1959): 54-56.
22. S. Dooley, S. H. Won, M. Chaos, J. Heyne, Y. Ju, F. L. Dryer, K. Kumar, C. J. Sung, H. Wang, M. A. Oehlschlaeger, R. J. Santoro, and T. A. Litzinger, "A jet fuel surrogate formulated by real fuel properties," *Combust. Flame*, vol. 157, no. 12, pp. 2333–2339, 2010.
23. Dooley, Stephen, et al. "The combustion kinetics of a synthetic paraffinic jet aviation fuel and a fundamentally formulated, experimentally validated surrogate fuel." *Combustion and flame* 159.10 (2012): 3014-3020.
24. Violi, A., et al. "Experimental formulation and kinetic model for JP-8 surrogate mixtures." *Combustion Science and Technology* 174.11-12 (2002): 399-417.
25. Edwards, Tim, et al. "Development of an experimental database and kinetic models for surrogate jet fuels." *45th AIAA Aerospace Sciences Meeting and Exhibit*. 2007.
26. Turns, Stephen R. *An introduction to combustion*. Vol. 499. New York: McGraw-hill, 1996.
27. Tsuji, Hiroshi. "Counterflow diffusion flames." *Progress in energy and combustion science* 8.2 (1982): 93-119.
28. F. E. Marble, "By," 1977.

29. Candel, Sebastien M., and Thierry J. Poinsot. "Flame stretch and the balance equation for the flame area." *Combustion Science and Technology* 70.1-3 (1990): 1-15.

30. Karlovitz, B., Denniston Jr, D. W., Knapschaefer, D. H., & Wells, F. E. (1953, January). Studies on Turbulent flames: A. Flame Propagation Across velocity gradients B. turbulence Measurement in flames. In Symposium (international) on combustion (Vol. 4, No. 1, pp. 613-620). Elsevier.

31. B. Karlovitz, D. W. Denniston, D. H. Knapschaefer, and F. E. Wells, "*Studies on Turbulent flames*." *Symp. Combust.*, vol. 4, no. 1, pp. 613–620, 1953.

32. C. K. Law, "*Dynamics of stretched flames*." *Symp. Combust.*, vol. 22, no. 1, pp. 1381–1402, 1989.

33. Mikolaitis, David W. "*The interaction of flame curvature and stretch, part 1: The concave premixed flame*." *Combustion and flame* 57.1 (1984): 25-31.

34. B. A. Williams, "*Sensitivity of calculated extinction strain rate to molecular formulation in nonpremixed counterflow flames*." Combustion and Flame, vol. 124, pp. 330–333, 2001.

35. G. Dixon-Lewis, "*Structure of laminar flames.*" Proceedings of the Combustion Institute, vol. 23, pp. 305–324, 1991

36. Williams, F. A., Combustion Theory. 1985: Addison-Wesley.

37. C.K. Law, Combustion Physics, Cambridge University Press, Cambridge, NY, 2006.

38. N. Peters, Turbulent Combustion, Cambridge University Press, Cambridge, England, 2000.

39. Power point presentation on Laminar diffusion flames: *Diffusion flamelet theory by Institu fur Technische Verbrennung.*

40. ANSYS Chemkin Theory Manual 17.0 (15151), Reaction Design: San Diego, 2015.

41. Colin William Curtis- “Combustion Characteristics of Thermally Stressed Hydrocarbon Fuels”. Master’s Thesis, 2016

42. Hongfa Huo 1, Xingjian Wang, Vigor Yang, *“A general study of counterflow diffusion flames at subcritical and supercritical conditions: Oxygen/hydrogen mixtures*”.

43. S. F. M. R.J. Kee, F.M. Rupley, J.A. Miller, M.E. Coltrin, J.F. Grcar, E. Meeks, H.K. Moffat, A.E. Lutz, G. Dixon-Lewis, M.D. Smooke, J. Warnatz, G.H. Evans, R.S. Larson, R.E. Mitchell, L.R. Petzold, W.C. Reynolds, M. Caracotsios, W.E. Stewart, P. Glarborg, C. Wan, “No Title,” *Chemkin Collect. Release 3.7.1, React. Des. Inc.*, 2003.

44. J. M. Smith, *Chemical Engineering Kinetics*. McGraw-Hill, 1981

45. A. T. Holley, Y. Dong, M. G. Andac, F. N. Egolfopoulos, and T. Edwards, “*Ignition and extinction of non-premixed flames of single-component liquid hydrocarbons, jet fuels, and their surrogate.*” *Proc. Combust. Inst.*, vol. 31 I, pp. 1205–1213, 2007.

46. S. H. Won, W. Sun, and Y. Ju, “*Kinetic effects of toluene blending on the extinction limit of n-decane diffusion flames*.” *Combust. Flame*, vol. 157, no. 3, pp. 411–420, 2010.

47. S. Humer, A. Frassoldati, S. Granata, T. Faravelli, E. Ranzi, R. Seiser, and K. Seshadri, “*Experimental and kinetic modeling study of combustion of JP-8, its 95 surrogates and reference components in laminar nonpremixed flows*.” *Proc. Combust. Inst.*, vol. 31 I, pp. 393–400, 2007.

48. C. K. Westbrook, W. J. Pitz, O. Herbinet, H. J. Curran, and E. J. Silke, “*A comprehensive detailed chemical kinetic reaction mechanism for combustion of n-alkane hydrocarbons from n-octane to n-hexadecane.*” *Combust. Flame*, vol. 156, no. 1, pp. 181–199, 2009.

49. Mehl M., W.J. Pitz, C.K. Westbrook, H.J. Curran, "Kinetic Modeling of Gasoline Surrogate Components and Mixtures Under Engine Conditions", Proceedings of the Combustion Institute 33:193-200 (2011).

50. "Chemical-Kinetic Mechanisms for Combustion Applications." *San Diego Mechanism web page, Mechanical and Aerospace Engineering (Combustion Research), University of California at San Diego (http://combustion.ucsd.edu)*.

51. Z. Luo, S. Som, S.M. Sarathy, M. Plomer, W.J. Pitz, D.E. Longman, T.F. Lu, "*Development and Validation of an n-Dodecane Skeletal Mechanism for Diesel Spray-Combustion Applications.*" Combustion and Theory Modeling, 18 (2) 187-203, 2014.

52. Won, Sang Hee, et al. "*A radical index for the determination of the chemical kinetic contribution to diffusion flame extinction of large hydrocarbon fuels*." *Combustion and Flame* 159.2 (2012): 541-551.

53. Dryer, Frederick L., et al. "Interpreting chemical kinetics from complex reaction–advection–diffusion systems: modeling of flow reactors and related experiments." *Progress in Energy and Combustion Science* 44 (2014): 19-39.

Appendix

Sonic Nozzles:

Sonic nozzles were used to control the volumetric flow rates of the nitrogen and air. Pressure regulators were used to monitor the flow rates of the gases. Each sonic nozzle was calibrated according to a certain pressure range. Four nozzles were used to control nitrogen blend, nitrogen vaporizer, nitrogen co-flow for shielding the flame against the surroundings, and air flow.

Sonic nozzles for controlling N_2 blend (SN#4)

Psi	L/min
20	0.156547
30	0.205308
40	0.254375
50	0.304526
60	0.355544
70	0.40219
80	0.45283
90	0.500626
100	0.551583
110	0.598504
120	0.648026
130	0.705882

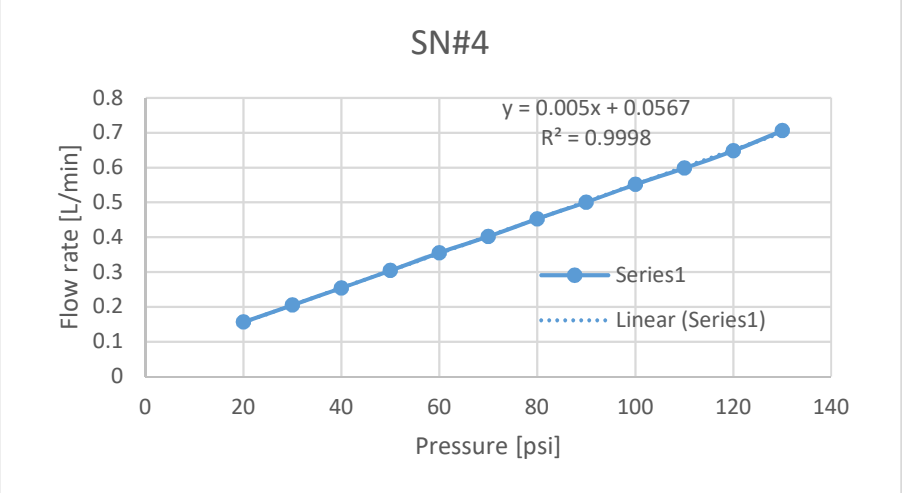

Sonic nozzles for controlling N_2 vaporizer (SN#7)

Psi	L/min
10	0.562207
20	0.801544
30	1.029552
40	1.263897

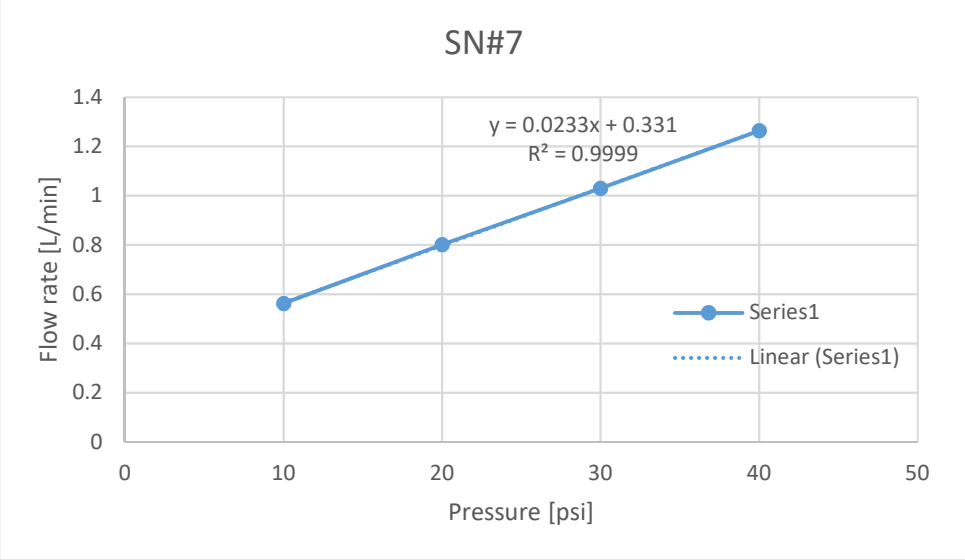

Sonic nozzles for controlling air flow (SN#9)

Psi	L/min
20	1.210762
30	1.585903
40	1.962923
50	2.3306
60	2.715615
70	3.081312
80	3.378167
90	3.782837

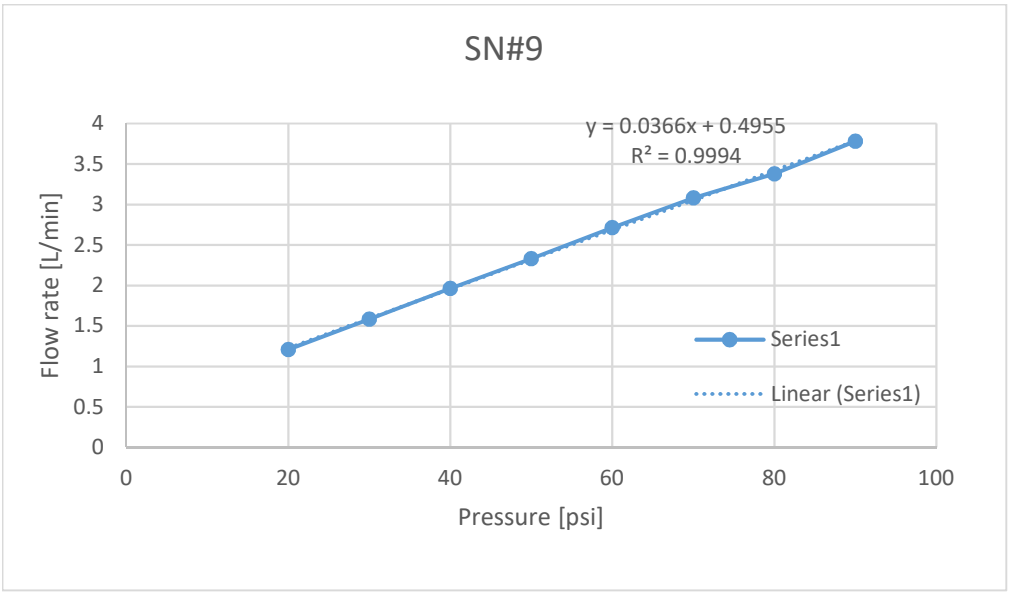

Temperature distribution profile of reactor

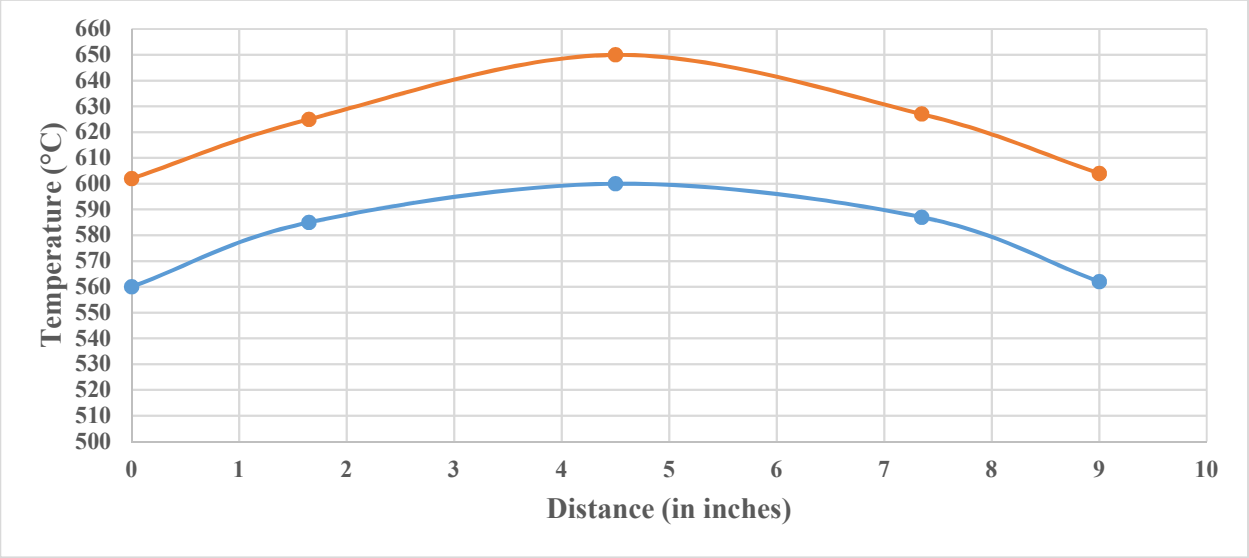

Orange denotes the temperature of the reactor when kept at 650 C, blue represents the profile when reactor temperature is 600 C. The profile was generated when there was no drop in temperature at the measured points.

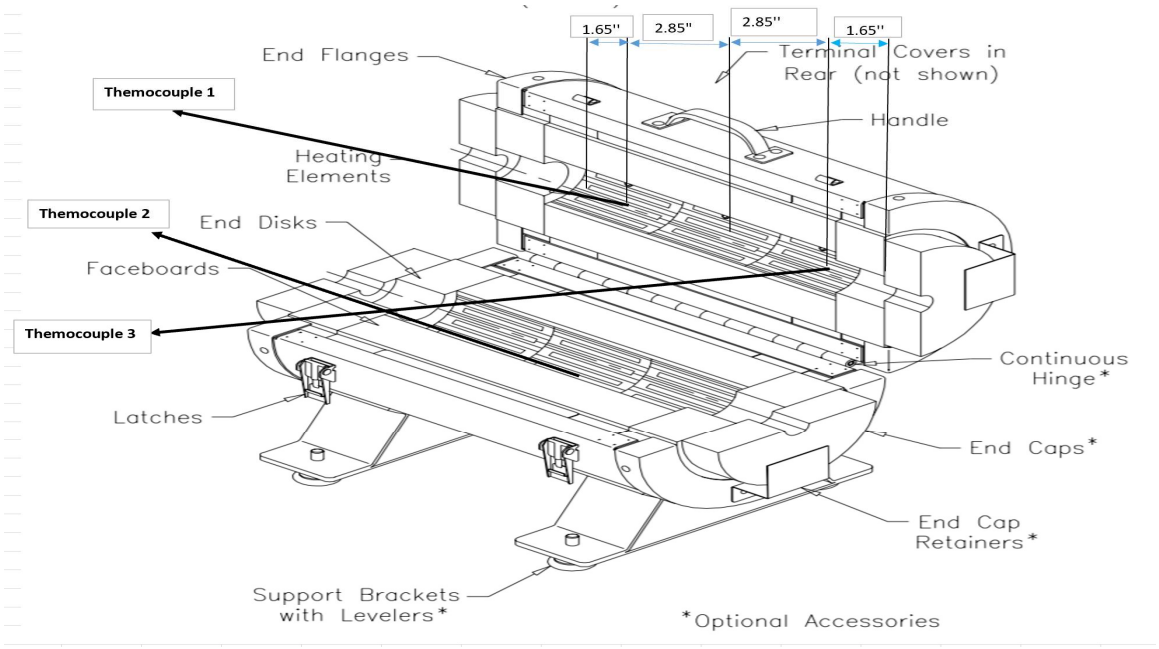

Composition of stressed n-heptane at **600 °C** and various pressures using GC/FID, and a residence time of 14.71 secs.

At 13.6 atm

Species	Mass fraction
Methane	0.000471159
Ethane	0.001771404
Ethyne	0.001513384
Propene	0.001891511
n-butane	0.001885869
n-pentane	0.001218527
Cylcohexene	0.001482345
C7-olefin	0.001601806
n-heptane	0.983778937
Methylcylcohexane	0.001092016

At 50 atm

Species	Mass fraction
Ethene	0.001442994
Ethane	0.005443135
Ethyne	0.006199558
Propane	0.009860246
isobutane	0.00639600
n-butane	0.010483201
Trans-2-butene	0.005967249
n-pentane	0.00737380
2-methyl-1,3-butadiene	0.001062296
1-hexene	0.0042049
Cyclohexene	0.001352488
C7-olefin	0.001391218
n-heptane	0.937732238
Methylcyclohexane	0.001069127

At 100 atm

Species	Mass fraction
Ethene	0.004690402
Ethane	0.012956311
Propene	0.018768037
Propane	0.03078072
isobutane	0.022499675
n-butane	0.029837706
2,2-dimethylpropane	0.023222923
cis-2-butene	0.001212567
isopentane	0.004347904
n-pentane	0.021064665
trans-2-pentene	0.004882923
1-hexene	0.010664466
n-hexane	0.001098978
cyclohexene	0.001241413
C7-olefin	0.001289702
n-heptane	0.811441608

At 150 atm

Species	Mass fraction
Methane	0.003565426
Ethane	0.007009246
Ethyne	0.014261535
Propene	0.020031898
Propane	0.018932191
n-butane	0.019871498
2,2-dimethylpropane	0.018754687
n-pentane	0.014865711
trans-2-pentene	0.003806315
1-hexene	0.007504699
cyclohexene	0.00137916
C7-olefin	0.001405293
n-heptane	0.868612343

At 170 atm

Species	Mass fraction
Ethene	0.004854001
Ethane	0.009803124
Propene	0.019926063
Propane	0.0317833
isobutane	0.02800274
n-butane	0.031790617
2,2-dimethylpropane	0.031185687
cis-2-butene	0.00188719
3-methyl-1-butene	0.001452083
n-pentane	0.024285698
trans-2-pentene	0.007349625
Cis-2-pentene	0.001266651
1-hexene	0.011814226
n-hexane	0.00219844
cyclohexene	0.00131207
C7-olefin	0.001364913
1-heptene	0.001254837
n-heptane	0.785309915
2-methyl-2-hexene	0.001036477
2,3-dimethyl-2-pentene	0.001038382
3-methylheptane	0.001083953

Composition of stressed n-heptane at **650 °C** and various pressures using GC/FID, and a residence time of 14.71 secs.

At 50 atm

Species	Mass fraction
Methane	0.004266
Ethane	0.015721
Ethyne	0.015843
Propane	0.022031
isobutane	0.012713
n-butane	0.020882
2,2-dimethyl propane	0.00996
n-pentane	0.01343
1-hexene	0.006861
Cylcohexene	0.001278
C7-olefin	0.001311
n-heptane	0.875705

At 100 atm

Species	Mass fraction
Ethene	0.005729
Ethane	0.015556
Ethyne	0.019795
Propane	0.027838
isobutane	0.019259
n-butane	0.02431
2,2-dimethylpropane	0.015974
cis-2-butene	0.001228
n-pentane	0.016795
trans-2-pentene	0.003894
1-hexene	0.010408
n-hexane	0.001036
cyclohexene	0.001194
c7-olefin	0.00126
1-heptene	0.001398
n-heptane	0.827161
2-methyl-2-hexene	0.001156
3-ethylhexane	0.006007

At 150 atm

Species	Mass fraction
Methane	0.003881
Ethane	0.010836
Ethyne	0.019298
Propane	0.041977
isobutane	0.03443
n-butane	0.05469
2,2-dimthylpropane	0.049759
cis-2-butene	0.006441
3-methyl-1-butene	0.00513
isopentane	0.001988
1,4-pentadiene	0.005211
n-pentane	0.046367
trans-2-pentene	0.017467
cis-2-pentene	0.004692
3-methyl-1,2-butadiene	0.002676
1,2-pentadiene	0.001204
3-methyl-1-pentene	0.00106
1-hexene	0.023956
n-hexane	0.005963
trans-3-hexene	0.002209
cis-2-hexene	0.001283
methylcyclopentane	0.001798
cyclohexene	0.001457
c7-olefin	0.001567
1-heptene	0.002995
c7-olefin	0.001461
n-heptane	0.645442
2-methyl-2-hexene	0.001998
Trans-2-methyl-3-hexene	0.001113
3-methylheptane	0.001655

At 170 atm

Species	Mass fraction
Methane	0.012824
Ethene	0.00149
Ethane	0.019898
Ethyne	0.044387
Propene	0.005592
Propane	0.06016
isobutane	0.05646
isobutene	0.006628
n-butane	0.054355
2,2-dimethypropane	0.055312
cis-2-butene	0.006022
3-methyl-1-butene	0.004646
n-pentane	0.039652
trans-2-pentene	0.01559
cis-2-pentene	0.003858
3-methyl-1,2-butadiene	0.002165
1-hexene	0.020058
n-hexane	0.006055
trans-3-hexene	0.001827
cis-2-hexene	0.001057
methylcyclopentane	0.001341
cyclohexene	0.00139
c7-olefin	0.001513
1-heptene	0.002702
c7-olefin	0.00134
n-heptane	0.567864
2-methyl-2-hexene	0.001835
Trans-2-methyl-3-hexene	0.001035
2,3-dimethyl-2-pentene	0.001202
3-methylheptane	0.001741